Cell Reports

Article

Dendritic Cells and Microglia Have Non-redundant Functions in the Inflamed Brain with Protective Effects of Type 1 cDCs

Graphical Abstract

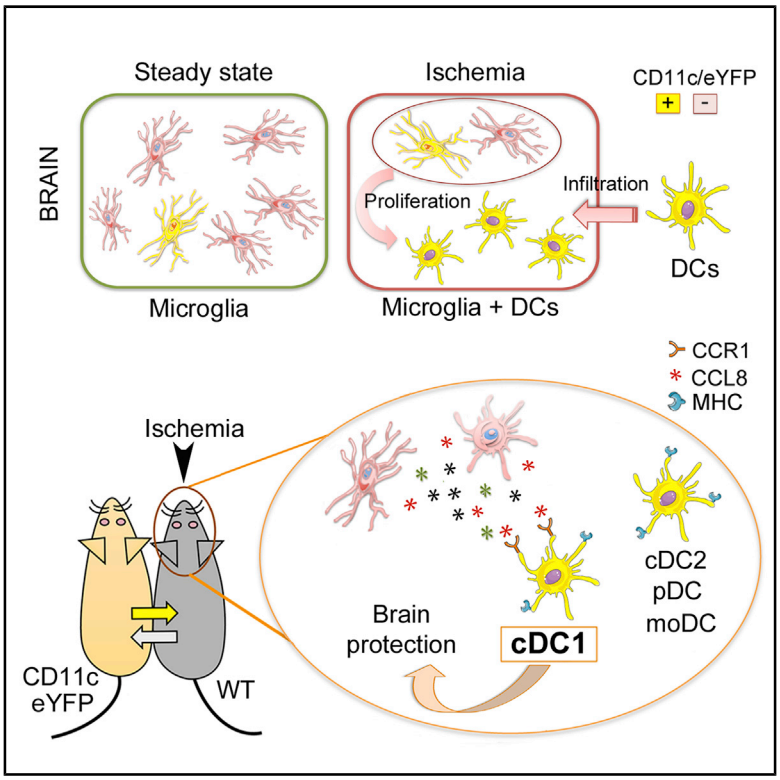

Highlights

- Microglia and DCs have distinct transcriptional profiles and functions in ischemia
- DCs excel over microglia in antigen presentation upon brain ischemia
- Ischemic microglia release chemokines attracting DCs, in particular cDC1 through CCR1
- cDC1 exert beneficial effects in brain ischemia

Authors

Mattia Gallizioli, Francesc Miró-Mur, Amaia Otxoa-de-Amezaga, ..., Carlos del Fresno, David Sancho, Anna M. Planas

Correspondence

anna.planas@iibb.csic.es

In Brief

CD11c$^+$ dendritic cells infiltrate the brain after ischemic injury and share some features with microglia. Gallizioli et al. show that dendritic cells exhibit a transcriptional profile different from microglia and excel in antigen presentation. Microglia attract different DC subsets via chemokines, especially cDC1 that exert beneficial functions in cerebral ischemia.

Gallizioli et al., 2020, Cell Reports *33*, 108291
October 20, 2020
https://doi.org/10.1016/j.celrep.2020.108291

CellPress

Cell Reports

CellPress
OPEN ACCESS

Article

Dendritic Cells and Microglia Have Non-redundant Functions in the Inflamed Brain with Protective Effects of Type 1 cDCs

Mattia Gallizioli,[1,2] Francesc Miró-Mur,[2,3] Amaia Otxoa-de-Amezaga,[1,2] Roger Cugota,[1,7] Angélica Salas-Perdomo,[1,3] Carles Justicia,[1,2] Vanessa H. Brait,[2,8] Francisca Ruiz-Jaén,[1,2] Maria Arbaizar-Rovirosa,[1,2] Jordi Pedragosa,[1,2] Ester Bonfill-Teixidor,[1,9] Mathias Gelderblom,[4] Tim Magnus,[4] Eva Cano,[5] Carlos del Fresno,[6] David Sancho,[6] and Anna M. Planas[1,2,10,*]

[1]Department of Brain Ischemia and Neurodegeneration, Institut d'Investigacions Biomèdiques de Barcelona (IIBB), Consejo Superior de Investigaciones Científicas (CSIC), Barcelona 08036, Spain
[2]Area of Neurosciences, Institut d'Investigacions Biomèdiques August Pi i Sunyer (IDIBAPS), Barcelona 08036, Spain
[3]Fundació Clínic, Barcelona 08036, Spain
[4]Department of Neurology, University Medical Center Hamburg-Eppendorf, Hamburg 20251, Germany
[5]Neuroinflammation Unit, Unidad Funcional de Investigación de Enfermedades Crónicas, Instituto de Salud Carlos III, Majadahonda, Madrid 28222, Spain
[6]Centro Nacional de Investigaciones Cardiovasculares (CNIC), Madrid 28029, Spain
[7]Present address: Institute of Neuroimmunology and Multiple Sclerosis Research, University Medical Center Göttingen, Göttingen, Germany
[8]Present address: The Florey Institute of Neuroscience and Mental Health, University of Melbourne, Parkville, Victoria, Australia
[9]Present address: Gene Expression and Cancer Team, Vall d'Hebron Institute of Oncology (VHIO), Barcelona, Spain
[10]Lead Contact
*Correspondence: anna.planas@iibb.csic.es
https://doi.org/10.1016/j.celrep.2020.108291

SUMMARY

Brain CD11c$^+$ cells share features with microglia and dendritic cells (DCs). Sterile inflammation increases brain CD11c$^+$ cells, but their phenotype, origin, and functions remain largely unknown. We report that, after cerebral ischemia, microglia attract DCs to the inflamed brain, and astroglia produce Flt3 ligand, supporting development and expansion of CD11c$^+$ cells. CD11c$^+$ cells in the inflamed brain are a complex population derived from proliferating microglia and infiltrating DCs, including a major subset of OX40L$^+$ conventional cDC2, and also cDC1, plasmacytoid, and monocyte-derived DCs. Despite sharing certain morphological features and markers, CD11c$^+$ microglia and DCs display differential expression of pattern recognition receptors and chemokine receptors. DCs excel CD11c$^-$ and CD11c$^+$ microglia in the capacity to present antigen through MHCI and MHCII. Of note, cDC1s protect from brain injury after ischemia. We thus reveal aspects of the dynamics and functions of brain DCs in the regulation of inflammation and immunity.

INTRODUCTION

Dendritic cells (DCs) are a heterogeneous population of cells in phenotype and origin, with tissue-specific features (Schlitzer et al., 2015). On the basis of ontogeny and function, DCs are classified as conventional DCs (cDCs) and plasmacytoid DCs (pDCs) under steady state. A further classification of cDCs is based on the expression of mutually exclusive markers: either XCR1 and DNGR-1 (*Clec9a*) (cDC1 lineage) or CD11b^{hi} and SIRPα (cDC2 lineage) (Guilliams et al., 2014). Fate-mapping studies demonstrated the existence of a DC hematopoietic lineage by identifying a common DNGR-1$^+$ DC precursor unable to generate monocytes and able to generate cDC1s and cDC2s to a different extent (Schraml et al., 2013). Inflammatory conditions induce the generation of inflammatory DCs (iDCs) that may derive from monocytes (Domínguez and Ardavín, 2010), but their origin is still unclear. DCs capture and present antigens, and their role is critical not only for mounting adaptive immune responses against invading pathogens but also for establishing tolerance to self-antigens under steady state. DCs traffic between tissues and lymphoid organs through the lymphatic system or they access different compartments through the blood vessels. Despite specific anatomic features of the central nervous system (CNS) (Ransohoff and Engelhardt, 2012), DCs are found surrounding the brain parenchyma, in brain regions proximal to the cerebrospinal fluid (CSF), and zones with an incomplete blood-brain barrier (i.e., at the frontline of interaction between brain and periphery). These regions comprise the leptomeninges, ventricles, choroid plexus, circumventricular organs, and rostral migratory pathway (Anandasabapathy et al., 2011; Bulloch et al., 2008; D'Agostino et al., 2012; Mohammad et al., 2014). Notably, cross-presenting cDC1s are found within meningeal/choroid plexus CD11c$^+$ cells in steady state (Anandasabapathy et al., 2011; Quintana et al., 2015). Besides these specific

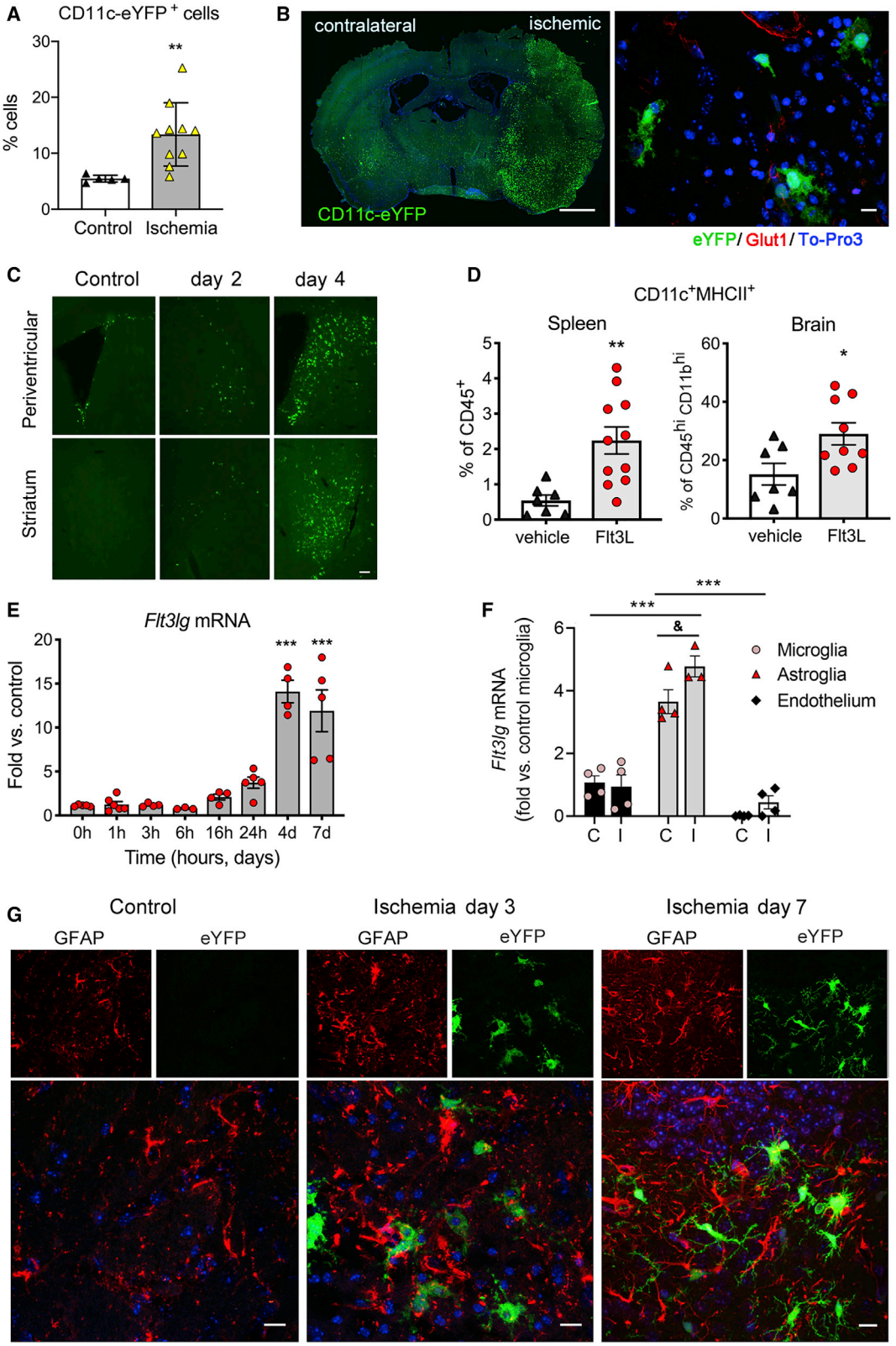

(legend on next page)

locations, CD11c$^+$ cells are rarely found in adult brain parenchyma under physiological conditions. However, their presence increases in the aged brain (Kaunzner et al., 2012) and under neuroinflammatory and neuropathological conditions, including infection, cancer, autoimmunity, seizures, neurodegenerative diseases, and stroke (Clarkson et al., 2012; D'Agostino et al., 2012; Ludewig et al., 2016).

Stroke causes acute sterile inflammation due to necrotic neural cell death triggered by sudden interruption of blood supply to certain brain regions (Chamorro et al., 2012, 2016; Dirnagl et al., 1999; Iadecola and Alexander, 2001; Iadecola and Anrather, 2011). CD11c$^+$ cell number increases in brain parenchyma in rodent models of ischemic stroke (Felger et al., 2010; Kostulas et al., 2002; Prodinger et al., 2011). Although some studies suggested that these cells may be microglia derived (Dando et al., 2016; Reichmann et al., 2002), a previous study demonstrated that about 50% of the CD11c$^+$ cells found in the ischemic brain infiltrated from the periphery (Felger et al., 2010). However, knowledge about the phenotype and function of resident and infiltrating CD11c$^+$ cells in the inflamed brain is still very limited. The objective of this study was to gain insight into the features and functions of brain resident and infiltrating CD11c$^+$ cells in the inflamed brain using a stroke mouse model of transient middle cerebral artery occlusion (tMCAo), transcriptomic analysis, cell phenotyping, immune assays, and generation of parabiotic (PA) mice.

RESULTS

Ischemia Increases CD11c$^+$ Cells and Flt3L Expression in Brain

Cerebral ischemia increased CD11c$^+$ cell number in the injured brain of CD11c-eYFP transgenic mice (Figure 1A), particularly at day 4 (Figures 1B and 1C), concurring with previous results (Felger et al., 2010). Fms-related tyrosine kinase 3 ligand (Flt3L) is an important growth factor for DC development and mobilization (Anandasabapathy et al., 2011; Coates et al., 2003; Guermonprez et al., 2013). Systemic Flt3L treatment increased CD11c$^+$ major histocompatibility complex class II (MHCII)$^+$ cells in spleen and ischemic brain (Figure 1D). The injured brain may provide support to CD11c$^+$ cells, as the brain expression of Flt3L mRNA (*Flt3lg*) increased peaking at day 4 post-ischemia (Figure 1E). To find out which brain cells produced Flt3L, we isolated microglia, astroglia, and endothelial cells from controls and 4 days post-ischemia (Figure S1). Astrocytes displayed the strongest *Flt3lg* mRNA expression, which increased after ischemia (Figure 1F). Furthermore, eYFP$^+$ cells were seen in the proximity of reactive astrocytes surrounding the ischemic core (Figure 1G).

Several studies suggested the existence of CD11c$^+$ microglia (Dando et al., 2016; Kamphuis et al., 2016), but the nature of brain CD11c$^+$ cells remains largely unknown. We checked whether cultured glial cells were able to express CD11c after stimulation. *Itgax* mRNA expression was induced from 8 to 48 h after IL-4 treatment, in agreement with a previous study (Butovsky et al., 2007), but not after lipopolysaccharide (LPS) (Figure S2A). In the ischemic tissue, some, but not all, eYFP$^+$ cells shared with microglia several morphological features, common markers, and proliferative capacity (Otxoa-de-Amezaga et al., 2019) (Figure S2B). However, after ischemia, sorted eYFP$^+$ cells showed lower mRNA expression than microglia of typical microglia genes (e.g., *Sall1, Tmem119*, *P2yr12*) (Figure S2C), suggesting differences between CD11c$^+$ cells and microglia.

Differential Transcriptional Signature of CD11c$^+$ Cells versus Microglia in the Ischemic Brain

We then compared the transcriptional profile of eYFP$^+$ cells and microglia sorted using fluorescence-activated cell sorting (FACS) 4 days post-ischemia (Figure 2A; Figure S3). For comparative purposes, we also obtained reference control microglia of non-ischemic mice. As control DCs, we sorted eYFP$^+$ cells from the spleen because of very small numbers in the brain at steady state. Comparative RNA sequencing (RNA-seq) showed that eYFP$^+$ cells of the ischemic brain display a gene expression profile distinct from microglia, both ischemic and control, and from spleen eYFP$^+$ cells (Figure 2B; Figures S4A and S4B). Enrichment analyses highlighted different biological processes

Figure 1. Ischemia Increases Brain CD11c-eYFP$^+$ Cells and Brain Flt3L

(A) Brain eYFP$^+$ cells increase 4 days post-ischemia in CD11c-eYFP mice. Flow cytometry values are percentages of viable cells. Mann-Whitney test, **p = 0.001, n = 5 controls, n = 10 ischemic mice.

(B) Left image: coronal brain section of a CD11c-eYFP mouse (n = 6) showing eYFP$^+$ cells (green) in the ischemic hemisphere (right); scale bar, 100 μm. Right image: higher magnification showing eYFP$^+$ cells in parenchyma; blood vessels (Glut1$^+$, red); nuclei (To-Pro3, blue); scale bar, 10 μm.

(C) In control, eYFP$^+$ cells are seen in ventricular region and rostral migratory pathway. After ischemia, eYFP$^+$ cells increase in the parenchyma. Scale bar, 30 μm.

(D) Mice received recombinant mouse Flt3L (10 μg/mouse) or vehicle subcutaneously (s.c.) for 7 days. Ischemia was induced 3 days after treatment onset, and tissue was studied by flow cytometry 4 days post-ischemia. Flt3L increased the percentage of CD11c$^+$MHCII$^+$ cells in spleen (Mann-Whitney test, **p = 0.001, n = 7 vehicle, n = 11 Flt3L) and ischemic brain (Mann-Whitney test, *p = 0.02, n = 7 vehicle, n = 9 Flt3L). Values are CD11c$^+$MHCII$^+$ cells expressed as percentages of CD45$^+$ cells or CD45^{hi}CD11b^{hi} cells.

(E) Brain Flt3L mRNA (*Flt3lg*) expression increases after ischemia (h, hours; d, days). One-way ANOVA and Dunnett's multiple comparison test, ***p < 0.001 versus control, n = 3–6 mice per time point.

(F) *Flt3g* mRNA in microglia, astroglia, and endothelial cells sorted from control and ischemic brains (day 4) (n = 3 or 4 samples per cell type and condition). Values are expressed as fold increase versus control microglia. Astrocytes show the highest *Flt3lg* mRNA expression versus microglia (***p = 0.0003) and endothelial cells (***p < 0.0001), and microglia show higher expression than endothelial cells (two-way ANOVA, p < 0.001, Sidak's multiple-comparisons test, ***p = 0.004). Ischemia 'I' increases astrocyte *Flt3lg* mRNA vs. control 'C' ($^{\&}$p = 0.049).

(G) Confocal microscope brain images of CD11c-eYFP mice (n = 3–6 mice per group). eYFP$^+$ cells (green) are located near reactive GFAP$^+$ astrocytes (red) at infarct periphery. Scale bar, 10 μm. Bars show mean ± SEM and symbols are values per mouse.

See also Figures S1 and S2.

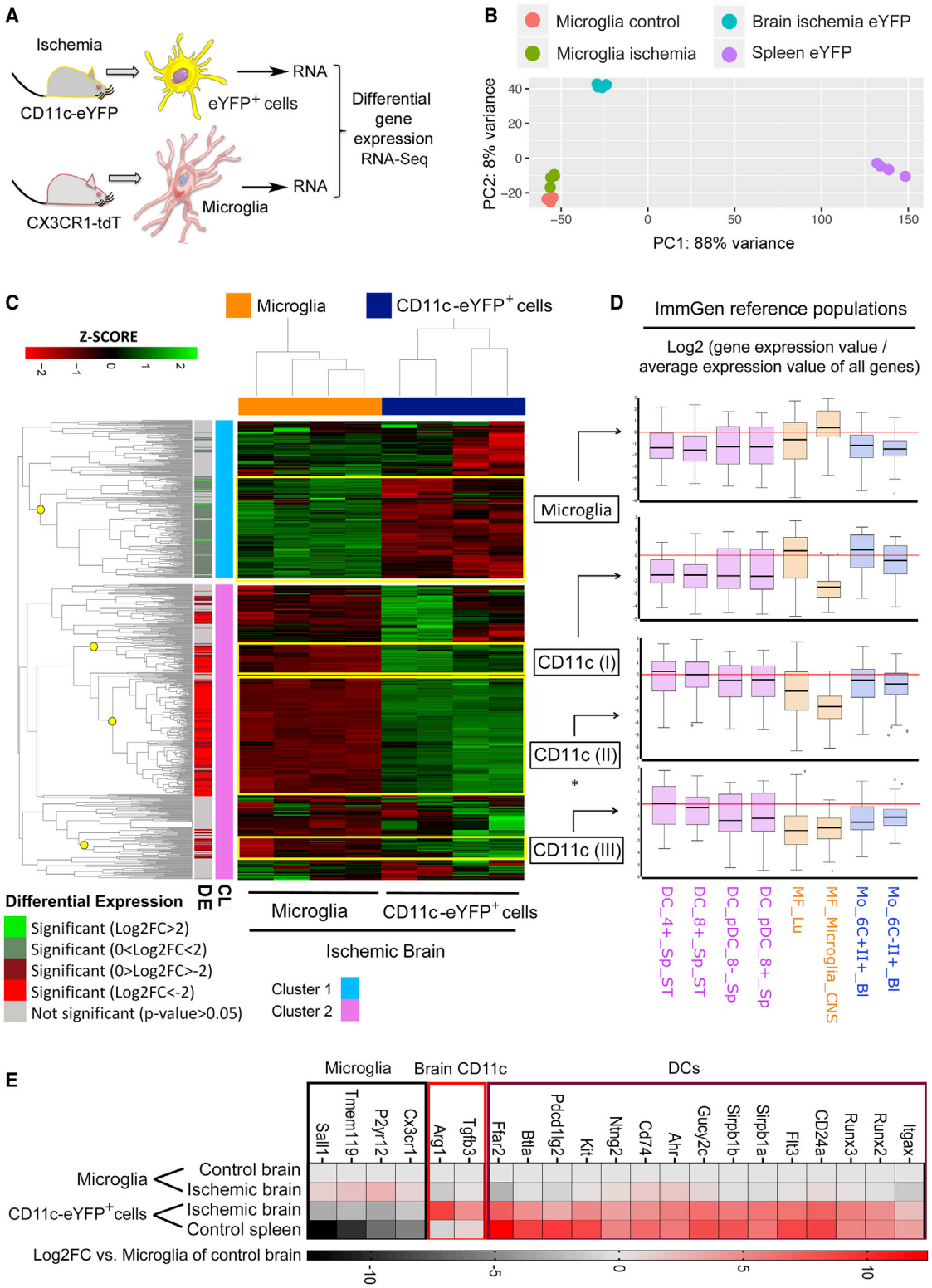

Figure 2. Differential Gene Expression between CD11c$^+$ Cells and Microglia of the Ischemic Mouse Brain

(A) RNA-seq of FACS-sorted microglia and eYFP$^+$ cells from CX3CR1cre^{ERT2}:Rosa26-tdT mice and CD11c-eYFP mice, respectively, 4 days post-ischemia. We also obtained microglia from control CX3CR1cre^{ERT2}:Rosa26-tdT mice and eYFP$^+$ cells from spleen of CD11c-eYFP control mice (n = 4 mice per group).

(B) Principal component analysis illustrates the unsupervised sample distribution.

(legend continued on next page)

in each of these cell groups and showed a differential transcriptional signature in eYFP$^+$ cells versus microglia in the ischemic brain tissue. We found 202 pathways enriched in eYFP$^+$ cells compared with microglia but only 21 pathways enriched in microglia compared with eYFP$^+$ cells. The fact that only a few pathways were enriched in microglia versus eYFP$^+$ cells suggested that microglial genes could be expressed in the eYFP$^+$ population too. Functional annotation clustering (Table S1) highlighted functions overrepresented in eYFP$^+$ cells versus microglia, such as antigen presentation and immune responses (Figure S4C). Microglia displayed overrepresentation of genes related to neural functions, such as γ-aminobutyric acid neurotransmission, neuropeptides, and synaptic vesicles, among others, suggesting specific microglial-neuronal interactions that are less prominent or absent in CD11c$^+$ cells.

We then compared the transcriptomic data with reference cell population expression profiles defined by the ImmGen project (ImmGen Consortium, 2016; Miller et al., 2012) using differential gene clustering analysis. We selected eight myeloid cell reference populations defined by ImmGen (https://www.immgen.org/). We compared gene expression in those populations in a pairwise manner to identify genes with the highest differential expression in each ImmGen population. Then we compared the expression of those sets of genes in our samples (Figures 2C and 2D). To validate this process, we checked that our control samples showed correspondence to the appropriate ImmGen populations (Figure S5). Gene expression data in microglia and eYFP$^+$ cells of the ischemic brain (Figure 2C) were compared with the ImmGen populations (Figure 2D). Gene clustering analysis revealed subclusters of differentially expressed genes in our samples, with high representation among reference microglia, lung macrophages and Ly6C$^+$ monocytic blood population, and splenic DC populations.

For validation purposes, we selected several genes differentially expressed between CD11c$^+$ cells and microglia of the ischemic brain and conducted a qRT-PCR study in FACS-sorted eYFP$^+$ cells and microglia obtained from independent groups of mice (Figure 2E). eYFP$^+$ cells showed higher expression than microglia of typical DC genes, such as *Runx3*, *Runx2*, and *Kit*. Furthermore, expression of typical microglial markers was comparatively lower in the eYFP$^+$ cells. The selected group of genes clearly separated microglia genes from DC genes, as illustrated in the volcano plot (Figure S4D). Notably, among the selected genes, *Tgfb3* and *Arg1* were overrepresented only in CD11c$^+$ cells of the ischemic brain and not microglia or spleen CD11c$^+$ cells. Altogether the results suggest that the ischemic brain tissue displays a complex population of CD11c$^+$ cells, including cells with features of cDCs and cells with brain-specific features, which are distinctive from previously described canonical DC populations.

CD11c$^+$ Cells in the Ischemic Brain Include Microglia and Infiltrating DCs

We then characterized CD11c$^+$ cells by flow cytometry using the widely used definition of mouse microglia as CD45^{lo}CD11b$^+$ cells, distinct from peripheral myeloid cells that are CD45^{hi}CD11b$^+$ (Ford et al., 1995). Under steady-state conditions the majority of brain eYFP$^+$ cells were CD45^{lo}CD11b$^+$, with only a low proportion of CD45^{hi} cells (Figure 3A). In another group of control CD11c-eYFP mice, we dissected out the choroid plexus and meninges separating those regions from the brain parenchyma and studied the eYFP$^+$ cells using flow cytometry. Most eYFP$^+$ cells in the brain parenchyma were CD45^{lo}CD11b$^+$ microglial cells (95% ± 1%, n = 4 hemispheres, n = 2 mice), whereas eYFP$^+$ cells in choroid plexus and meninges were CD45^{hi} (43% ± 12%) or CD45^{lo} (25% ± 4%) (Figures 3B and 3C). Four days post-ischemia, the proportion of CD45^{hi} cells within brain eYFP$^+$ cells increased to about one half, whereas the other half corresponded to CD45^{lo}CD11b$^+$ cells (Figures 3D and 3E), showing a mixed population of brain resident and infiltrating CD11c$^+$ cells. CD45^{lo}CD11b$^+$eYFP$^+$ cells corresponded to 6.9% ± 2.2% (mean ± SD, n = 3) of the total CD45^{lo}CD11b$^+$ microglia in the injured brain hemisphere.

Infiltrating DCs Excel in Antigen Presentation Compared with Microglia

For functional information about CD11c$^+$ cells and microglia in the ischemic brain, we focused on antigen presentation. The expression of genes related to antigen presentation increased in the brain tissue after ischemia, as illustrated by the expression of *Cd74* mRNA encoding MHCII invariant chain, which peaked at day 4 (Figure 4A). The RNA-seq study showed that expression of MHCII genes was overrepresented in eYFP$^+$ cells compared with microglia in the injured tissue 4 days post-ischemia (Figure 4B, upper heatmap). Likewise, mRNA expression of MHCII complex transactivator *Ciita*, *Cd74*, and genes encoding immunomodulatory molecules, such as *Tnfsf4* (OX40L, CD252), *Dpp4*, *Btla*, and *Pdcd1lg2* (PD-L2), and the costimulatory molecules *Cd80* and *Cd40*, was higher in eYFP$^+$ cells than microglia (Figure 4B, lower heatmap). eYFP$^+$ cells were frequent in myelin-rich areas of the

(C and D) Comparison of transcriptomic data of ischemic microglia and eYFP$^+$ cells (C) with ImmGen reference cell population expression profiles using differential gene clustering analysis. Data represented as boxplots (D). Heatmap of differential gene expression between microglia and eYFP$^+$ cells of ischemic tissue (C). Unsupervised clustering analysis differentiated microglia from eYFP$^+$ cells by genes upregulated (green) or downregulated (red) in each group. We selected four subclusters (yellow squares in heatmap) by significance and magnitude (fold change) of their differential expression.

(D) Gene subclusters overrepresented in eYFP$^+$ cells (I, II, and III with 53, 203, and 34 genes, respectively) and one microglia subcluster (with 177 genes) were used for comparison with eight ImmGen reference populations: four types of spleen (Sp) DCs, lung (Lu) macrophages (MF), microglia, and blood (Bl) monocytes (Mo, Ly6C$^+$, and Ly6C$^-$). Asterisk indicates that because of limitations in the ImmGen My Geneset tool, only the 200 most differentially expressed genes (non-corrected p value < 0.01) of the CD11c (II) subcluster were included in the analysis.

(E) We selected 20 genes differentially expressed in eYFP$^+$ cells versus microglia for RT-PCR validation with microglia and eYFP$^+$ cells sorted from independent groups of ischemic mice (n = 4 per group). We grouped the genes according to their overrepresentation population as "Microglia," CD11c$^+$ cells (indicated as "DCs") in spleen and ischemic brain CD11c$^+$ cells, and "Brain CD11c" in ischemic brain CD11c$^+$ cells only. Multiple comparison t test between brain CD11c$^+$ versus microglia cells showed statistically significant differences for all genes (Holm-Sidak, $\alpha = 0.05$).

See also Figures S3–S5 and Table S1.

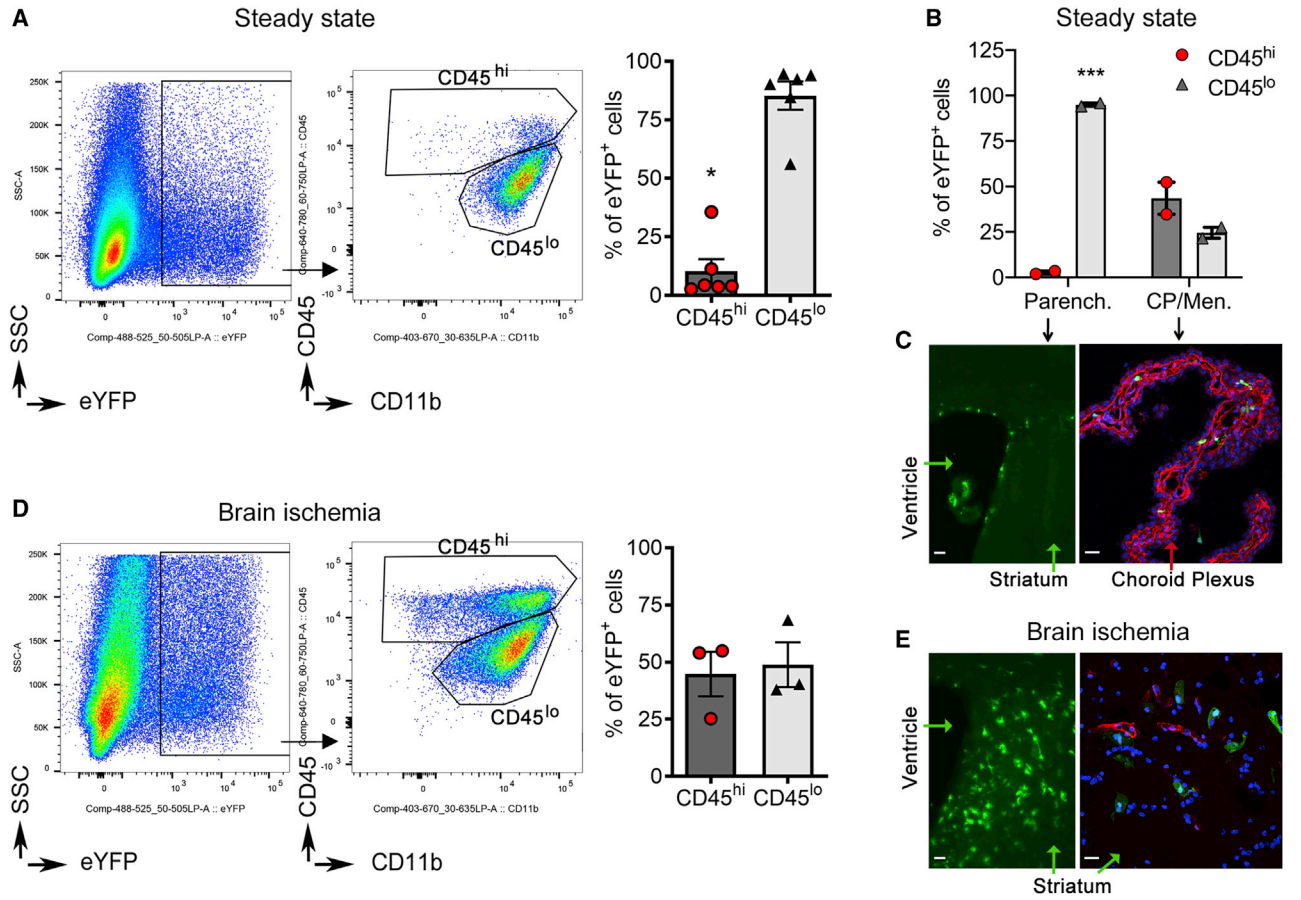

Figure 3. CD11c$^+$ Cells in the Inflamed Brain Parenchyma Include Microglia and Infiltrating DCs

(A) Most eYFP$^+$ cells are CD45^{lo}CD11b$^+$ at steady state (Wilcoxon matched-pairs signed rank test, *p = 0.03, n = 6 eYFP-CD11c mice).

(B) Separation of choroid plexus and meninges (CP/Men.) from brain parenchyma (Parench.) confirmed that most eYFP$^+$ cells in brain parenchyma were CD45^{lo}CD11b$^+$ cells (n = 2 mice, two brain hemispheres processed separately for each mouse; two-way ANOVA, ***p = 0.0003), whereas CD45^{hi}CD11b$^+$eYFP$^+$ cells were found in choroid plexus and meninges.

(C) Images of eYFP$^+$ cells (green) in each region shown in (B).

(D) Flow cytometry of brain tissue 4 days post-ischemia shows that approximately half of the brain eYFP$^+$ cells are CD45^{hi} and the other half are CD45^{lo}CD11b$^+$ microglia (n = 3 mice).

(E) Representative images of ischemic tissue show abundant eYFP$^+$ cells (green) in parenchyma. Images on the right-hand side in (C) and (E) are immunostained with pan-laminin (red) and nuclei (To-Pro3, blue). In graphs, bars are mean ± SEM, and symbols show individual values per mouse. Scale bar, 20 μm.

injured tissue, where they may interact with myelinated nerve fibers (Figure 4C). Among the CD11c$^+$ cell population, CD45^{hi} cells expressed notably higher levels of MHCII than CD45^{lo}CD11b$^+$ microglia (Figure 4D), suggesting that the subset of CD11c$^+$ microglia has limited capacity to present antigen through MHCII.

We then asked whether antigen presentation capacity was different in CD11c$^+$ cells after separating between CD45^{hi} and CD45^{lo} cells. CD80 expression was rather low (<1% of the respective parent populations; data not shown). However, approximately 20% of CD45^{hi}CD11c$^+$ cells expressed the immunostimulatory molecule OX40L, whereas fewer than 5% of CD45^{lo}CD11c$^+$ microglia did, and we did not detect this molecule in CD45^{lo}CD11c$^-$ microglia (Figure 4E). Among the CD45^{hi}CD11b$^+$CD11c$^+$ cells, we detected the presence of a major population of cDC2 (CD172$^+$) and a smaller population of cDC1 cells (XCR1$^+$) (Figure 4F; Figure S6). cDC2 were positive for immunomodulatory molecule OX40L, whereas cDC1 were not (Figure 4G).

For a functional assessment, we studied the capacity of CD45^{lo} cells, including CD11c$^-$ and CD11c$^+$ microglia, and CD45^{hi}CD11c$^+$ cells sorted from the ischemic brain tissue to induce T cell proliferation. To this end, we used OTII transgenic mice with CD4$^+$ T cells specific for ovalbumin (OVA) 323–339 peptide. We co-cultured these CD4$^+$ T cells in the presence or absence of CD45^{lo}CD11b$^+$eYFP$^-$ microglia, CD45^{lo}CD11b$^+$eYFP$^+$ microglia, or CD45^{hi}CD11b$^+$eYFP$^+$ cells sorted from the brain of CD11c-eYFP mice 4 days after ischemia and exposed to OVA peptide (chicken OVA 323–339 peptide). Irrespective of CD11c expression, microglia showed a reduced capacity to stimulate T cell proliferation compared with CD45^{hi}CD11b$^+$eYFP$^+$ cells (Figure 4H). For class I-restricted

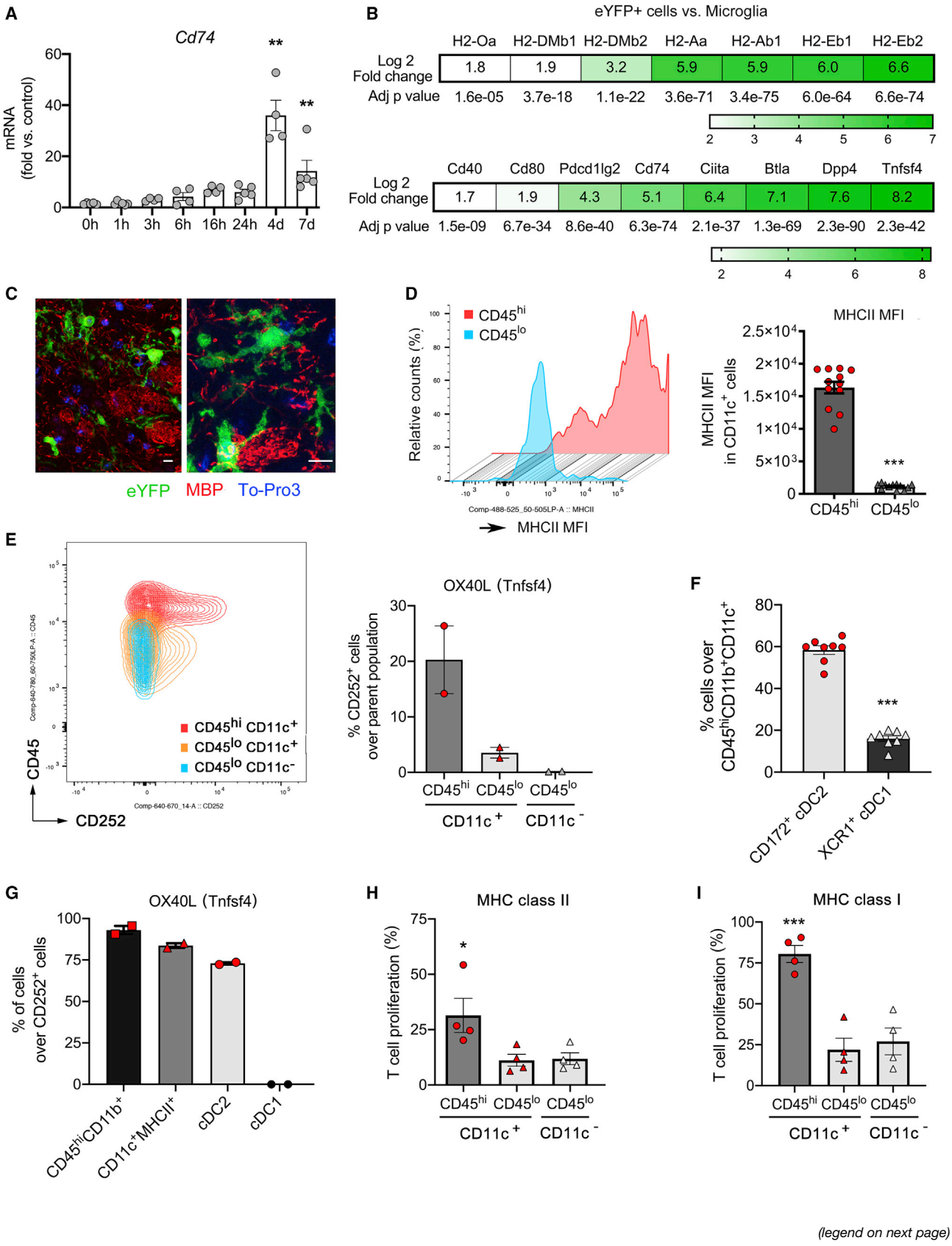

(legend on next page)

antigen presentation, we used OTI transgenic mice with $CD8^+$ T cells specific for the OVA 257–264 peptide (SIINFEKL). We obtained $CD8^+$ T cells from these mice and co-cultured them with $CD45^{lo}CD11b^+eYFP^-$ microglia, $CD45^{lo}CD11b^+eYFP^+$ microglia, or $CD45^{hi}CD11b^+eYFP^+$ cells (Figure S7) previously exposed to a pulse of SIINFEKL peptide. Again, $CD45^{hi}CD11b^+eYFP^+$ cells were the most efficient population to induce $CD8^+$ T cell proliferation (Figure 4I). Therefore, the expression of CD11c in a subset of microglia of the adult brain does not confer a higher capacity to induce adaptive immune responses, while infiltrating $CD45^{hi}CD11b^+eYFP^+$ cells represent a bona fide DC population of cells that excel in their antigen presenting capacity.

Selective Characterization of Infiltrating DCs with Parabiosis Studies

To identify $CD11c^+$ cells trafficking from the periphery to the inflamed brain we generated PA pairs by joining the circulation of wild-type (WT) mice and transgenic CD11c-eYFP littermates (Figure 5A). After 3 weeks of parabiosis, we detected a few $eYFP^+$ cells located mainly in the leptomeningeal zone and choroid plexus, while being absent from the brain parenchyma (Figures 5Bi–5Biii). Therefore, the choroid plexus/meninges contain a dynamic $CD11c^+$ population of cells capable of interchanging with the periphery in steady state. In contrast, $CD11c^+$ cells located in the brain parenchyma are a brain-resident population. In other groups of PA mice, we induced cerebral ischemia in the WT mouse of each PA pair (Figure 5A). Four days post-ischemia, we detected $eYFP^+$ cells in the ischemic brain parenchyma (Figure 5Biv–5Bvii), leptomeninges, and choroid plexus (Figure 5Bvi) of the PA WT mice. Flow cytometry (Figure S8) confirmed the very small number of $eYFP^+$ cells in the brain of the PA WT mice in steady state and the increased number following ischemia (Figure 5C). Most infiltrating $eYFP^+$ cells were $CD45^{hi}CD11b^+$ cells (mean ± SD 84.3% ± 4.4%, n = 5).

We then compared the transcriptomic profile of brain $eYFP^+$ cells sorted from the PA ischemic WT mice (infiltrating $eYFP^+$ cells) with that of microglia sorted from the brain of ischemic mice. In parallel, we sorted $eYFP^+$ cells from the brain of ischemic CD11c-eYFP mice (total brain $eYFP^+$ cells) for comparative purposes. Principal component analysis separated infiltrating cells (PA eYFP) from microglia and from total $eYFP^+$ cells (Figure 5D). Comparison of the transcriptomic data of our cells with that of ImmGen reference cell populations (Figure 5E) showed a subcluster of genes similar to lung macrophages, and subclusters with similarities to spleen DCs and $Ly6C^+$ blood monocytes. The top 50 genes overrepresented in PA $eYFP^+$ cells versus microglia in the ischemic brain are shown in Table S2. Infiltrating PA $eYFP^+$ cells showed certain differences versus microglia in the expression of genes encoding C-type lectin receptors (CLRs) and endosomal Toll-like receptors (TLRs). A wide repertoire of pattern recognition receptors (PRRs) of the CLR family, including MCL (*Clec4d*), DNGR-1 (*Clec9a*), DCAR (*Clec4b1*), MINCLE (*Clec4e*), DECTIN-2 (*Clec4n*), CD301 (*Clec10a*), CD371 (*Clec12a*), OCILRP2 (*Clec2i*), ZNF705A (*Clec4a1*), and DECTIN-1 (*Clec7a*) were overrepresented in infiltrating PA $eYFP^+$ cells versus microglia (Figure 5F). In contrast, microglia overexpressed brain-associated C-type lectin (BACL, *Clec2l*), whose expression is high in brain tissue (Lysenko et al., 2013). Expression of *Tlr7*, *Tlr3*, and *Tlr12* was higher in microglia, whereas PA $eYFP^+$ cells showed upregulation of *Tlr8*. These results illustrate cellular specialization in innate sensing and show a better overall equipment in infiltrating DCs. Enriched pathways in PA $eYFP^+$ cells versus microglia highlighted immune functions in the former (Table S3). Enrichment analysis identified overrepresentation of functions related to neuronal development and differentiation, as well as terms and pathways related to cell proliferation, in ischemic microglia compared with $eYFP^+$ cells of PA ischemic WT mice (Table S3). Accordingly, we did not detect $Ki67^+$ $eYFP^+$ cells in the ischemic brain of PA WT mice (data not shown), whereas we found it after ischemia in non-PA CD11c-eYFP mice (see Figure S2B). Gene set enrichment analysis (GSEA) also identified overrepresentation in microglia of genes involved in the cell division cycle, including G2/M checkpoint, mitotic spindle assembly, cell cycle-related targets of E2F transcription factors, and genes associated with spermatogenesis (including genes with neuroendocrine secretory functions and genes involved in cell proliferation) (Figure 5G; Figure S9). Moreover, GSEA highlighted an IFN-α signature induced by ischemia

Figure 4. Infiltrating $CD11c^+$ Cells Surpass Microglia in Antigen Presentation Capacity

(A) MHCII antigen-associated *Cd74* mRNA expression in brain tissue at different time points (from immediately after ischemia (0 h) to 7 days; n = 3–7 mice per time point, Kruskal-Wallis test and Dunn's multiple-comparisons test, $^{**}p < 0.01$).

(B) Differential gene expression between $eYFP^+$ cells and microglia sorted from ischemic brain shows overrepresentation of genes involved in antigen presentation, co-stimulation, and immunomodulation in $eYFP^+$ cells.

(C) $eYFP^+$ cells (green) in myelin-rich areas (MBP, red) 7 days post-ischemia. Nuclei are stained with To-Pro3 (blue). Scale bar, 10 μm.

(D) Among $CD11c^+CD11b^+$ cells in ischemic brain, $CD45^{hi}$ cells display higher MHCII expression than $CD45^{lo}$ cells, as showed by the MHCII mean fluorescence intensity (MFI) (paired t test, $^{***}p < 0.001$, n = 12 mice).

(E) OX40L (CD252, *Tnfsf4*) expression is high in $eYFP^+CD45^{hi}$ DCs, but not $CD45^{lo}$ microglia 4 days post-ischemia (n = 2 mice).

(F) $CD45^{hi}CD11b^+CD11c^+$ cells 4 days post-ischemia comprise different subsets of DCs, including $CD172^+$ cDC2 cells and $XCR1^+$ cDC1 cells (Wilcoxon matched-pairs signed rank test, $^{**}p = 0.008$, n = 8 mice).

(G) cDC2 cells express OX40L, whereas cDC1 do not.

(H) Proliferation of OTII T cells stimulated with OVA peptide 323–339 in the presence of either $eYFP^+CD45^{hi}$ DCs, $eYFP^+CD45^{lo}CD11b^+$ microglia, or $eYFP^-CD45^{lo}CD11b^+$ microglia obtained by FACS from the brain of CD11c-eYFP mice 4 days post-ischemia (n = 4 mice). One-way ANOVA with a repeated-measure design and Holmes-Sidak multiple-comparisons test showed higher T cell proliferation induced by $CD45^{hi}CD11c^+$ DCs versus $CD11c^+$ microglia ($^*p = 0.032$) or $CD11c^-$ microglia ($^*p = 0.028$).

(I) Proliferation of OTI CD8 T cells exposed to cells (obtained as in H) that were previously pulsed with SIINFEKL peptide. Again $CD45^{hi}CD11c^+$ cells showed higher capacity than microglia to induce $CD8^+$ T cell proliferation. Statistical analysis as in (G), $^{***}p < 0.0001$ for both $CD11c^+$ and $CD11c^-$ microglia, n = 4 experiments performed with cells obtained from different ischemic mice. Bars show mean ± SEM and symbols show individual values per each mouse.

See also Figures S6 and S7.

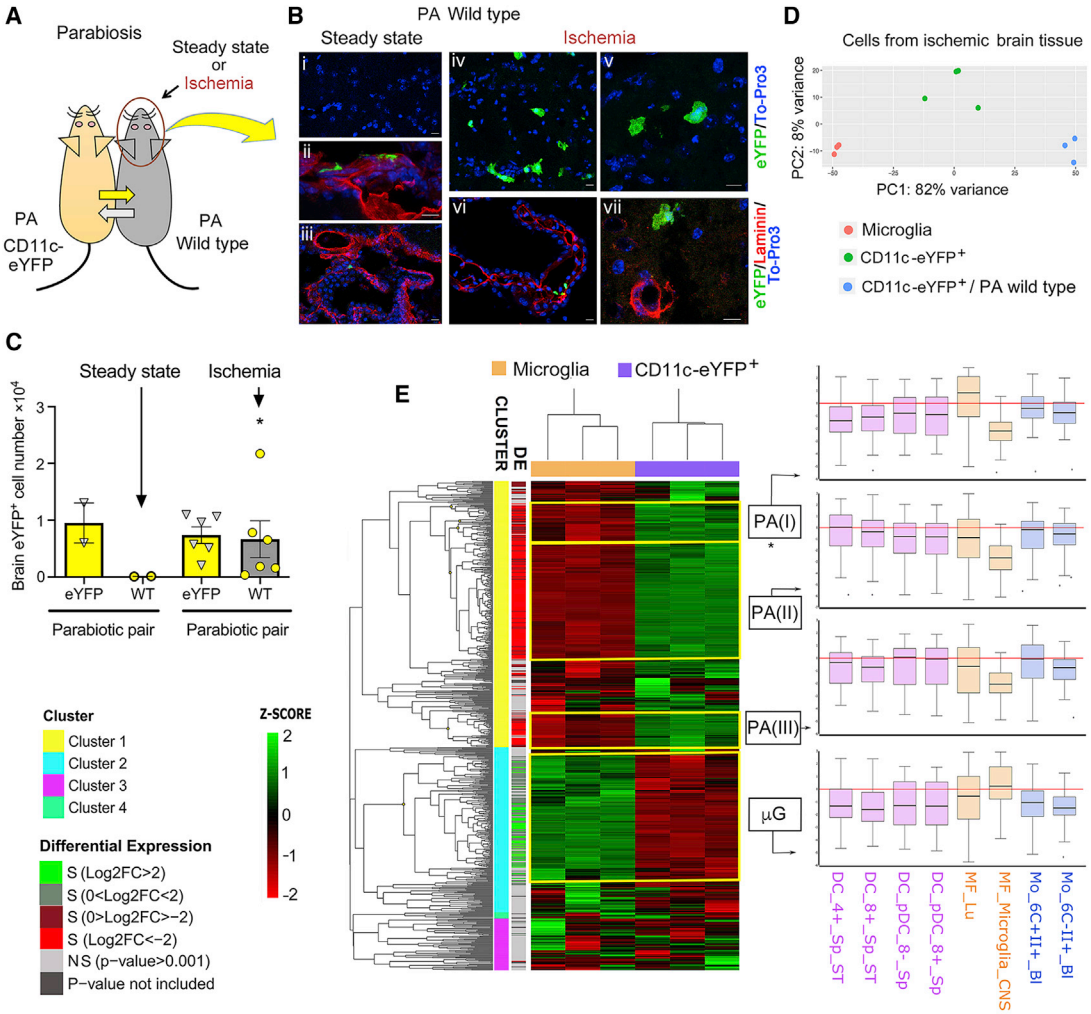

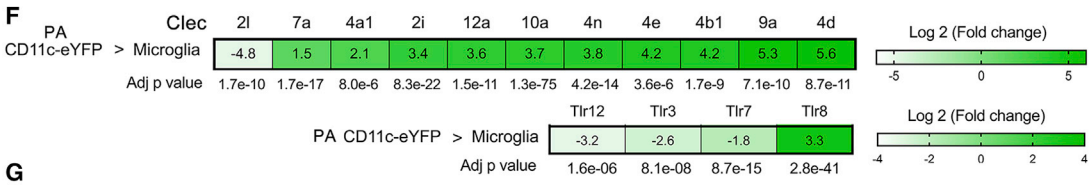

G

	NAME	SIZE	NES	NOM p-val	FDR q-val	RANK AT MAX
PA eYFP+	ROS PATHWAY	47	0.698	0.0	0.0	2860
	OXIDATIVE_PHOSPHORYLATION	196	0.588	0.0	0.0	4470
	CHOLESTEROL_HOMEOSTASIS	73	0.482	0.0	0.024	1869
	IL2_STAT5_SIGNALING	193	0.458	0.00	0.035	1435
	ANGIOGENESIS	33	0.441	0.04	0.040	1046
Microglia	INTERFERON_ALPHA_RESPONSE	90	-0.564	0.0	0.007	3315
	G2M_CHECKPOINT	193	-0.551	0.0	0.004	3184
	MITOTIC_SPINDLE	198	-0.505	0.0	0.010	2539
	E2F_TARGETS	196	-0.500	0.0	0.009	3763
	TGF_BETA_SIGNALING	53	-0.450	0.02	0.029	1975
	SPERMATOGENESIS	110	-0.421	0.0	0.047	2146

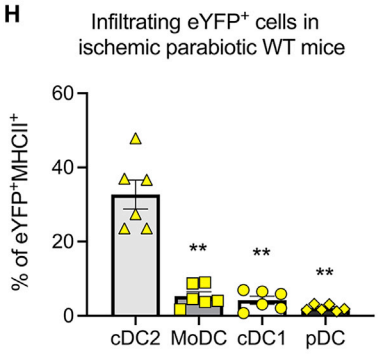

(legend on next page)

in microglia only, and it identified upregulation of TGF-β signaling in microglia but not in infiltrating eYFP$^+$ cells (Figure 5G; Figure S9). In contrast, features of the infiltrating eYFP$^+$ cells included an active response to reactive oxygen species, high oxidative and lipidic metabolism, STAT5-dependent signaling, and angiogenesis (Figure 5G; Figure S9).

We then studied the identity of peripheral eYFP$^+$ cells infiltrating the ischemic brain tissue of WT PA mice by phenotyping DC subsets by flow cytometry. Infiltrating eYFP$^+$ cells included a major population of CD172$^+$ cDC2, and less abundant XCR1$^+$ cDC1, pDCs, and monocyte-derived DCs (moDCs) (Figure 5H; gating strategy is shown in Figure S8).

Chemoattraction of DCs to the Ischemic Brain

We investigated the signals that may attract peripheral DCs to the inflamed brain. The RNA-seq analysis of parabionts showed high overrepresentation of several genes encoding chemokine receptors in infiltrating eYFP$^+$ cells versus microglia of ischemic mice (Figure 6A). Of note, only the expression of atypical chemokine receptor 3 (*Ackr3* encoding for CXCR7) was higher in microglia than eYFP$^+$ cells (Figure 6A). We validated some of these chemokine receptor genes by RT-PCR in RNA of FACS-sorted cells obtained from independent groups of mice (Figure 6B). Notably, ischemia induced mRNA expression of chemokines binding those DC receptors at different time points (Figure 6C; Figure S10A). *Ccl5* and *Ccl8* mRNA expression was strongly induced 4 and 7 days post-ischemia. This time course was compatible with the time point of CD11c$^+$ cell accumulation (see Figure 1C). We isolated microglia, astrocytes, and endothelial cells from control brain tissue and 4 days post-ischemia to identify which brain cells express these chemokines. Ischemia upregulated *Ccl8* and *Ccl5* expression mainly in microglia (Figure 6D). To find out whether microglia contributed to DC infiltration to the ischemic brain tissue, we used a pharmacological strategy to deplete microglia. Given that microglial cell viability is CSF1R dependent, chronic treatment with the CSF1R inhibitor PLX5622 provided in the diet causes strong microglial depletion (Otxoa-de-Amezaga et al., 2019). The treatment reduced CD45^{hi}CD11c$^+$ cells expressing MHCII (i.e., infiltrating DCs), while it did not modify CD11c$^+$MHCII$^+$ cell numbers in the spleen (Figure 6E). Microglia depletion reduced the numbers of all DC subsets as follows: cell number values (mean ± SD) for PLX5622 diet versus control diet, respectively (n = 12 per group, Mann-Whitney test) are for cDC1, 370 ± 282 versus 1,509 ± 818 ($p = 0.007$); for cDC2, 8,223 ± 3,776 versus 18,277 ± 11,209 ($p = 0.012$); for moDCs, 960 ± 670 versus 1,869 ± 1,136 ($p = 0.033$); and for pDCs, 1,638 ± 1,306 versus 2,811 ± 1,054 ($p = 0.014$). This effect was attributable to the reduction of chemokine production in the ischemic brain tissue after microglia depletion (Figure 6F). cDC2, moDC, and pDC subsets were similarly affected by the absence of microglia, as the percentage over the parent population of CD11c$^+$MHCII$^+$ cells was similar between microglia-depleted and non-depleted groups. Of note, cDC1 showed a stronger reduction than the other DC subsets after microglia depletion (Figure 6E). Therefore, cDC1 recruitment to the ischemic brain appears to be particularly dependent on chemokines generated by microglia.

cDC1 Exert Protective Functions in Brain Ischemia

CCL8, CCL5, and CCL3 bind CCR1, suggesting that this receptor expressed in brain infiltrating DCs (see Figures 6A and 6B) could be involved in the migration of CD11c$^+$ cells to the

Figure 5. Characterization of Infiltrating CD11c$^+$ Cells Obtained from Parabiotic Mice

(A) Parabiotic (PA) pairs obtained by joining CD11c-eYFP mice with wild-type (WT) littermates. After 3 weeks we studied the brain of each pair (n = 4), or we induced brain ischemia in the WT mouse of each pair and studied the brain 4 days later (n = 11).

(B) Brain tissue immunofluorescence of PA WT mice in steady state (i–iii) (n = 2) and after ischemia (iv–vii) (n = 2) show eYFP$^+$ cells (green). Nuclei are stained with To-Pro3 (blue). Images (ii, iii, vi, and viii) are also stained with pan-laminin (red). In steady state, there are few eYFP$^+$ cells in the subpial space (ii) and choroid plexus (iii) but not in brain parenchyma (i) of the WT parabiont. eYFP$^+$ cells in meninges, choroid plexus (vi) and ischemic brain parenchyma (iv, v, and vii) of the ischemic WT parabiont. Scale bar, 10 μm.

(C) eYFP$^+$ cell number (flow cytometry) in brain of PA pairs. At steady state, the number of eYFP$^+$ cells (mean ± SD) in WT PA brain is small (117 ± 41 eYFP$^+$ cells, n = 2). Ischemia increases eYFP$^+$ cells in PA-WT brain (6,638 ± 7,955 eYFP$^+$ cells, n = 6) ($p = 0.03$, one-sample Wilcoxon test).

(D) Transcriptome analysis of eYFP$^+$ cells sorted from the ischemic brain of PA-WT mice (n = 3) or ischemic CD11c-eYFP mice (n = 4) and microglia (n = 3 per group). Principal component analysis shows sample distribution.

(E) Heatmap representation of differential genes upregulated (green) or downregulated (red) among microglia and infiltrating eYFP$^+$ cells from the PA-WT mice using 776 genes retrieved from the comparison with ImmGen reference cell populations. The representation includes 4 natural clusters found by unsupervised clustering: subclusters PA(I), PA(II), and PA(III) were upregulated in PA samples, and subcluster μG was upregulated in microglia. Subclusters contained 62, 185, 55, and 200 genes, respectively. The expression of genes included in each subcluster was checked on the ImmGen reference cell populations, and the generated boxplots are displayed in the figure. *This subcluster was generated by merging together the genes contained in three adjacent subclusters because of the small number of genes and similar expression profile in reference populations. Data in graphs are expressed as $\log_2$ (gene expression value/average expression value of all genes).

(F) Differential gene expression between CD11c-eYFP$^+$ cells sorted from PA WT mice and microglia after ischemia illustrates overrepresentation of genes encoding C-type lectin receptors (Clec) in infiltrating eYFP$^+$ cells versus microglia, with the exception of Clec2l higher in microglia. Endocytic TLRs also showed some differential expression between these cells.

(G) Table showing GSEA results. The top rows with positive enrichment score correspond to PA eYFP$^+$ cells and the bottom rows with negative enrichment score correspond to microglia. Only the pathways with a false discovery rate (FDR) of less than 5% are shown. "Size" is the number of gene sets enriched in each phenotype; NES, normalized enrichment score; NOM p-val, nominal p value; RANK AT MAX, position in the ranked list at which the maximum enrichment score occurred; ROS, reactive oxygen species.

(H) Flow cytometry of subpopulations of eYPF$^+$ DCs infiltrating the brain of ischemic WT mouse of each parabiotic pair (n = 6 pairs). Numbers of eYFP$^+$ cDC2 cells are higher than eYFP$^+$ cDC1 cells (**$p = 0.004$), eYFP$^+$ moDCs (**$p = 0.006$), and eYFP$^+$ pDCs (**$p = 0.002$) (one-way ANOVA with a repeated-measures design and Dunnett's multiple-comparisons test). Bars show group mean ± SEM and points are values per mouse.

All mice used in this figure were females. See also Figures S8 and S9 and Tables S2 and S3.

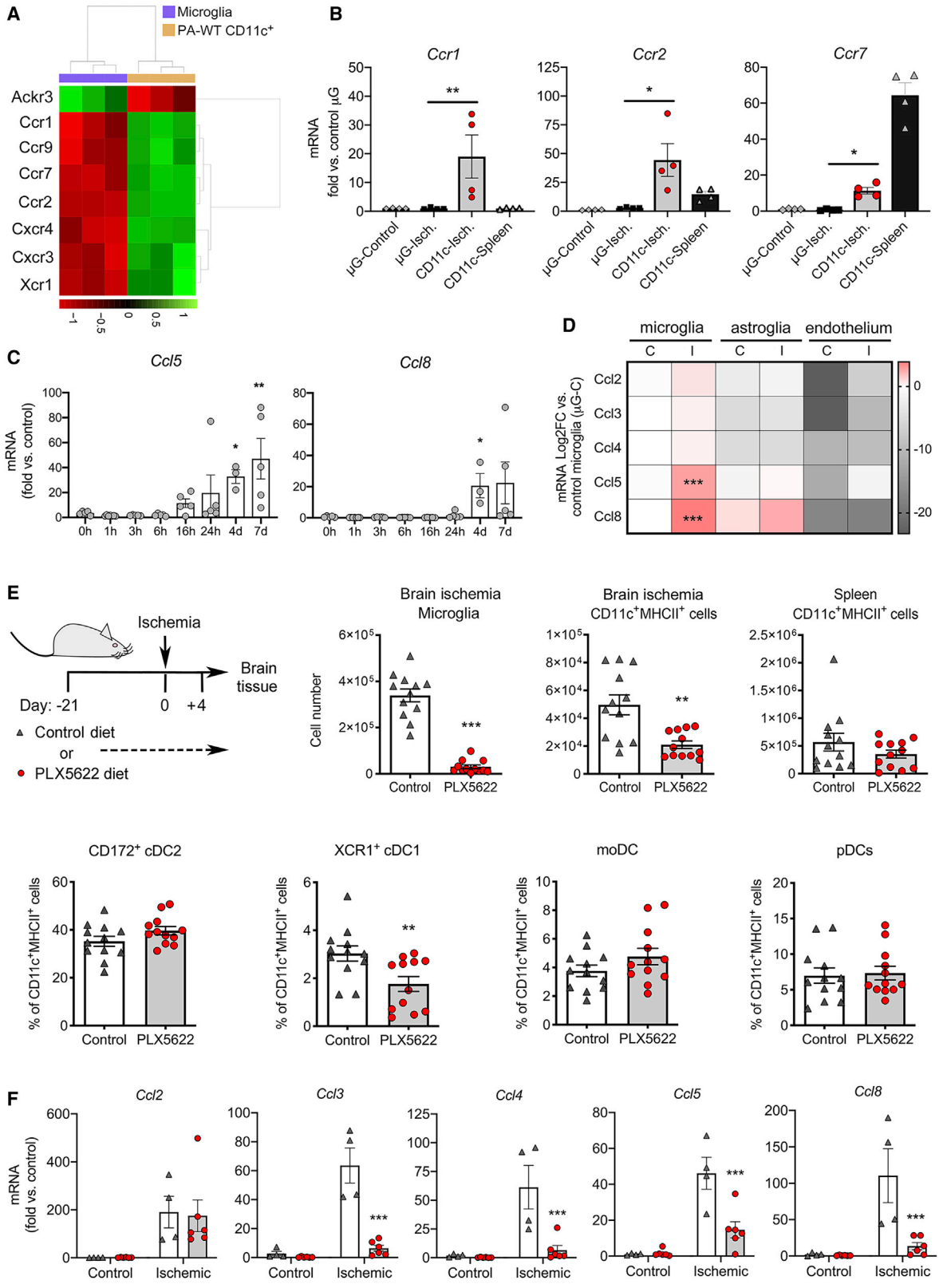

(legend on next page)

ischemic tissue. To test this possibility, we blocked CCR1 by systemic (intraperitoneal [i.p.]) administration of CCR1 antagonist J113863 (Amat et al., 2006) to WT mice (Figure 7A). The drug did not induce significant changes in infiltrating leukocytes, pDCs, moDCs, and CD172$^+$ cDC2 cells but reduced XCR1$^+$ cDC1 cell number (Figure 7B; Figure S10B). The neurological score and the sizes of the lesion were not different between groups before treatment, as assessed by MRI and behavioral tests 24 h post-ischemia, prior to drug administration. Drug treatment did not modify the size of the lesion versus the vehicle 4 days post-ischemia (Figure S10C). However, the neurological score worsened from day 1 to day 4 in the CCR1 antagonist group versus the vehicle group (Figure 7C), suggesting a beneficial effect of cDC1 in brain ischemia. cDC1 cell development requires the transcription factor BATF3 (Hildner et al., 2008). cDC1 cells are strongly reduced in *Batf3*$^{-/-}$ mice, and we did not detect these cells in the ischemic tissue of *Batf3*$^{-/-}$ mice (Figure 7D), whereas the other DC populations were not significantly affected (Figure 7D; Figure S10D). *Batf3*$^{-/-}$ mice showed larger infarctions and worse neurological deficits than WT mice (Figure 7E).

We verified that worse stroke outcome in *Batf3*$^{-/-}$ mice was not attributable to alterations in cerebrovascular anatomy such as the extent of collateral circulation (Figure S10E). To find out whether infiltrating hematopoietic cells contributed to the worse outcome of *Batf3*$^{-/-}$ mice, we generated chimeric mice by transplanting bone marrow of either *Batf3*$^{-/-}$ mice or WT (*Batf3*$^{+/+}$) mice to WT recipient mice (Figure 7F). After ischemia, lesion volume slightly increased from day 1 to day 4 in chimeric mice with *Batf3*$^{-/-}$ hematopoietic cells but not in mice with WT hematopoietic cells (Figure 7G). Accordingly, at day 4 post-ischemia, neurological function was worse in the mice with *Batf3*$^{-/-}$ hematopoietic cells (Figure 7G). Altogether these results support a beneficial effect of infiltrating cDC1s in brain ischemia.

DISCUSSION

We report that most CD11c$^+$ cells found in the mouse brain parenchyma in steady state are CD45^{lo}CD11b$^+$ microglia, whereas the choroid plexus and meninges display CD45^{hi}CD11c$^+$ cells that traffic from the periphery. CD11c$^+$ cells in the ischemic tissue originate from a complex mixture of DCs invading the inflamed brain and proliferating resident microglia, in line with a previous study (Felger et al., 2010). Our study further demonstrates that CD11c$^+$ microglia differ from DCs in the limited capacity of the former to present antigen and induce T cell proliferation. The population of microglial cells is heterogeneous and shows phenotypic and functional diversity (Silvin and Ginhoux, 2018). A CD11c$^+$ microglial subset is involved in myelinogenesis (Wlodarczyk et al., 2017), and several lines of evidence support specific functions and protective effects of CD11c$^+$ microglia (Benmamar-Badel et al., 2020). In our study both microglia and infiltrating CD11c$^+$ cells expressed genes involved in functions related to glial development and differentiation, whereas neuronal function was represented in microglia.

Necrotic cell death induced by ischemia generates danger-associated molecular patterns (DAMPs) and activation of innate immune receptors (Iadecola and Anrather, 2011). DAMPS can induce sterile inflammation through activation of various PRRs, including TLRs and certain CLRs (Gong et al., 2020). Immature DCs are tolerogenic, but they mature to immunostimulatory phenotypes after PRR activation. Brain infiltrating DCs showed a different CLR and TLR expression repertoire than microglia, suggesting cellular specialization in the recognition of danger signals in the injured brain. The transcriptomic analysis also showed overrepresentation of several chemokine receptors, such as *Ccr1* and *Ccr2*, in infiltrating CD11c$^+$ cells versus microglia, whereas only *Ackr3* expression was higher in microglia than infiltrating CD11c$^+$ cells. ACKR3, a scavenger of CXCL12, was previously found in microglia in which expression increased under inflammatory stimuli (Lipfert et al., 2013). Microglial cells seem to be instrumental for attraction of peripheral DCs to the inflamed brain by upregulating the expression of *Ccl5* and *Ccl8* mRNA. Accordingly, microglia depletion reduced ischemia-induced expression of chemokines in brain and attenuated DC infiltration, particularly of cDC1. Therefore, glial cells are critical for recruiting and maintaining DCs in the inflamed brain, as microglia generate DC chemoattractants and astrocytes produce Flt3L necessary to support DC viability (Coates et al., 2003; Guermonprez et al., 2013). Microglia depletion strongly reduced DC

Figure 6. CCR1-Mediated Chemoattraction of cDC1s

(A) Chemokine receptor genes overrepresented ($p < 0.001$, $\log_2$ fold change [FC] > 2) in infiltrating eYFP$^+$ cells of parabiotic (PA) WT ischemic mice versus microglia of ischemic mice (n = 3 mice per group).

(B) Validation by RT-PCR in microglia from control and ischemic brain (Isch; 4 days post-ischemia), CD11c$^+$ cells from ischemic brain, and spleen CD11c$^+$ cells (n = 4 per group). Kruskal-Wallis test and Dunn's multiple-comparisons test, *$p < 0.05$ and **$p < 0.01$.

(C) Brain *Ccl5* and *Ccl8* mRNA expression at different time points after ischemia (n = 3–7 mice per time point). Kruskal-Wallis test and Dunn's multiple-comparisons test, *$p < 0.05$ and **$p < 0.01$.

(D) Chemokine mRNA expression (RT-PCR) in microglia, astroglia, and endothelial cells sorted from control (C) or ischemic (I) brain (day 4) (n = 4 per group). Values are expressed as $\log_2$ fold change versus control microglia. Ischemia increased *Ccl8* and *Ccl5* mRNA expression mainly in microglia. Multiple-comparison t test, ***$p < 0.001$.

(E) WT mice received either diet with CSF1R inhibitor PLX5622 or control diet for 25 days (n = 12 mice per group). After 21 days of treatment, ischemia was induced, and brain was studied 4 days later using flow cytometry. PLX5622 severely depleted microglia and reduced the number of CD11c$^+$MHCII$^+$ infiltrating DCs in the ischemic brain but did not alter the number of spleen DCs. Mann-Whitney test, ***$p < 0.001$ and **$p = 0.002$. Microglia depletion specifically reduced the recruitment of cDC1 cells to ischemic tissue (Mann-Whitney test, **$p = 0.007$).

(F) Chemokine mRNA expression at day 4 in ischemic brain (striatum) of PLX5622-treated mice (n = 6) or controls (n = 4) (symbols as in 'E'). Although microglia depletion reduced the expression of *Ccl3* ($p < 0.0001$), *Ccl4* ($p = 0.0003$), *Ccl5* ($p = 0.0003$), and *Ccl8* ($p = 0.0006$) mRNA, it did not modify *Ccl2* mRNA ($p = 0.970$). Two-way ANOVA by treatment and ischemia effects, followed by Sidak's multiple-comparisons test; control tissue is corresponding contralateral non-ischemic hemisphere. Bars show group mean ± SEM and points are values per mouse.

See also Figure S10A.

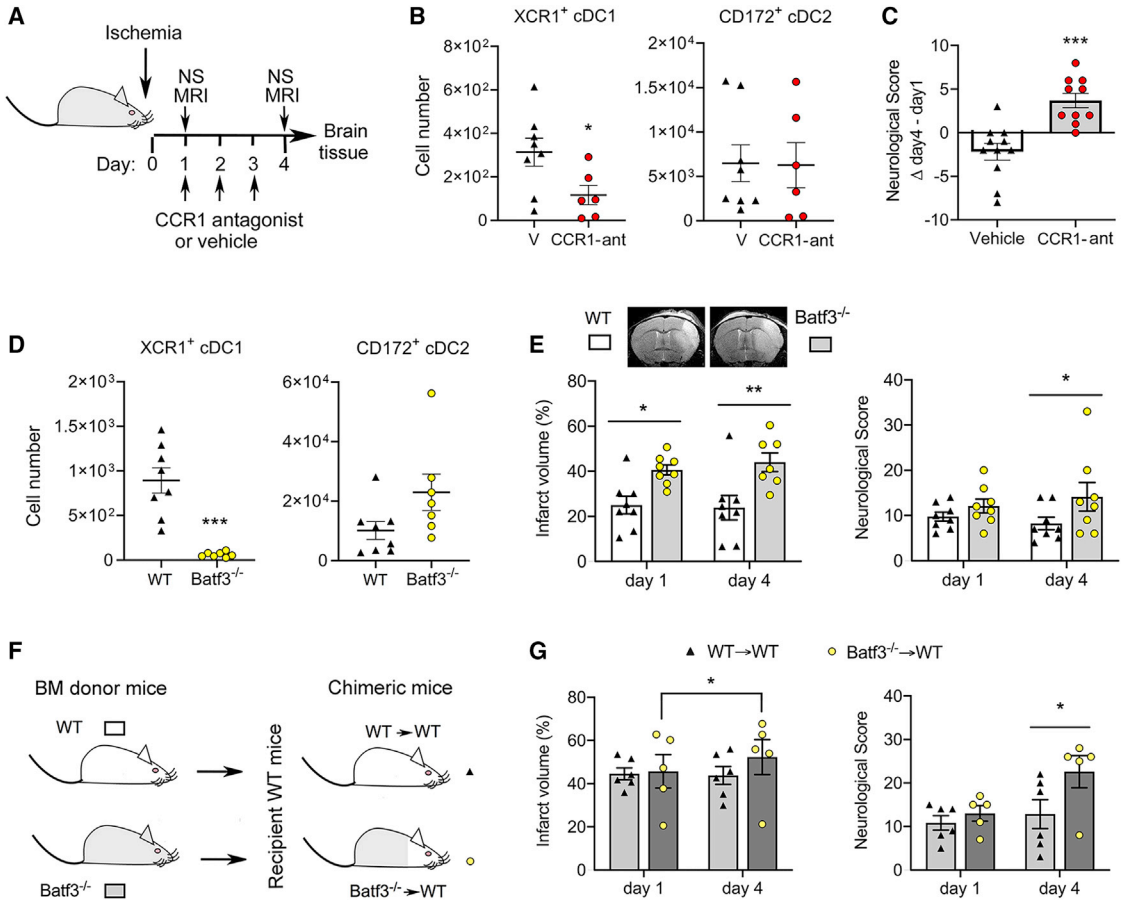

Figure 7. Protective Role of cDC1 in Brain Ischemia

(A) Daily administration of CCR1 antagonist J113863 (CCR1-ant) or the vehicle starting 1 day post-ischemia until day 3. We monitored the brain lesion using MRI and assessed the neurological function with a neuroscore (NS) (higher values indicate worse deficits). Brain tissue was studied at day 4 using flow cytometry.

(B) CCR1-ant (n = 6) did not affect cDC2 number but reduced cDC1 (n = 8) (Mann-Whitney test, ***p = 0.0007).

(C) Prior to drug treatment, the neurological score (mean ± SD; vehicle, 11.3 ± 5.0; CCR1-ant, 10.0 ± 5.1) was similar in both groups. Four mice per group died and were excluded. The neurological score worsened from day 1 to day 4 in the CCR1-ant group (n = 10) versus the vehicle group (n = 11) (Mann-Whitney test, ***p = 0.0002). "Δ day 4–day1" is the difference in NS between the two time points in the same mice.

(D and E) We induced ischemia in *Batf3*$^{-/-}$ mice (n = 8) and WT mice (n = 8) and studied the brain 4 days later (D). Batf3 deficiency depleted cDC1 cells and (E) increased MRI infarct volume. Two-way ANOVA by genotype and time point with a repeated-measures design; genotype effect, p = 0.005; Sidak's multiple-comparisons test showed significant differences between genotypes at both time points (*p = 0.018 and **p = 0.002). The NS was also worse in *Batf3*$^{-/-}$ mice than WT mice. Friedman test followed by Dunn's multiple-comparisons test, *p = 0.031.

(F) We generated chimeric mice by transplanting bone marrow (BM) of either *Batf3*$^{-/-}$ (n = 5) or WT (n = 6) donor mice to recipient WT mice. Chimeric mice with *Batf3*$^{-/-}$ BM lacked cDC1 cells in the spleen (<0.3% cDC1 over CD11c^{+}MHCII^{+} cells) compared with the mice with WT BM (10%–15% cDC1).

(G) After ischemia, mice with *Batf3*$^{-/-}$ BM show an increase in infarct volume from day 1 to 4 that is not detected in mice with WT BM (two-way ANOVA with repeated-measures design followed by Sidak's multiple-comparisons test, *p = 0.047). Accordingly, the NS is worse in the mice with *Batf3*$^{-/-}$ BM 4 days post-ischemia (Mann-Whitney test, *p = 0.037). Bars show group mean ± SEM and points are values per mouse.

See also Figures S10B–S10E.

infiltration but did not entirely abrogate it. It is plausible that other brain cells such as astrocytes or endothelial cells could participate in attracting DCs.

Different subsets of DCs display various immunomodulatory mechanisms to interact and shape T cell responses (Bourque and Hawiger, 2018). Compared with microglia, infiltrating CD11c^{+} cells overexpressed genes of typical co-stimulatory molecules *Cd80*, *Cd40*, and *Dpp4* (CD26) (Hatano et al., 2015; Ohnuma et al., 2008), and the immunomodulatory gene *Tnfsf4* (OX40L or CD252). OX40L binds OX40 on T cells to stimulate clonal expansion of effector and memory T cells (Croft et al., 2009), and it can induce regulatory T cell dysfunction (Jacquemin et al., 2018). Notably, in the ischemic brain, OX40L was expressed by cDC2 cells and not by other infiltrating DC populations or microglia. We previously demonstrated deleterious effects of cDC2s mediated by IL-17-driven innate immune responses that exacerbate the brain lesion after stroke (Gelderblom et al., 2018). In the present study DCs, but not CD11c^{-} and CD11c^{+} microglia, obtained from the ischemic brain were able to induce proliferation of CD4^{+} or CD8^{+} T cells. In other

neurological conditions, MHCI-restricted $CD8^+$ T cell priming is dependent on DCs (Malo et al., 2018). In experimental autoimmune encephalomyelitis (EAE), antigen presentation by peripheral DCs is necessary for reactivation of myelin oligodendrocyte glycoprotein (MOG)-reactive encephalitogenic T cells (Greter et al., 2005), and a population of cDCs samples and presents myelin antigens and is critical for licensing T cells to initiate neuroinflammation (Mundt et al., 2019). Wlodarczyk et al. (2014) specifically addressed the capacity of $CD11c^-$ and $CD11c^+$ microglia to present antigen versus infiltrating $CD11c^+$ cells in EAE. This study showed equivalent ability to induce proliferation of MOG-immunized $CD4^+$ T cells by CNS-resident $CD11c^+$ microglia or blood-derived $CD11c^+$ cells, but the former were unable to induce pathogenic T cell responses. Although it is possible that the disease-specific environment determined the maturation status of $CD11c^+$ microglia and shaped the capacity of these cells to interact with T cells, the different studies seem to agree in that $CD11c^+$ microglia has lower capacity of pathogenic T cell induction than infiltrating DCs.

We identified cDC1 among the infiltrating $CD11c^+$ cells and found expression of *Clec9a*, which may contribute to sensing necrotic cell death and modulating the inflammatory response (del Fresno et al., 2018; Sancho et al., 2009). Infiltration of cDC1 to the ischemic brain was, at least in part, dependent on CCR1, and cDC1s were protective in brain ischemia. cDC1 play critical roles in inducing T helper 1 and cytotoxic T cell immunity because of their capacity to cross-present antigen (Hildner et al., 2008). Moreover, cDC1 regulate complex innate immune responses (Janela et al., 2019; Del Fresno and Sancho, 2019) that may contribute to their effect on stroke outcome. Under pathological conditions, several lines of evidence support the participation of cDC1 in induction of tolerance mediated by promoting inducible Treg cells in several experimental settings (Coombes et al., 2007; Sun et al., 2007; Toubai et al., 2010; Khare et al., 2013; Arnold et al., 2019). This effect may be relevant for stroke outcome because Treg cells play critical immunomodulatory functions in brain ischemia and exert protective effects (Liesz et al., 2009). These results underscore the need to further investigate DC function in brain diseases because DC-based druggable targets might open new therapeutic avenues for neuroinflammatory conditions.

STAR★METHODS

Detailed methods are provided in the online version of this paper and include the following:

- KEY RESOURCES TABLE
- RESOURCE AVAILABILITY
  - Lead Contact
  - Materials Availability
  - Data and Code Availability
- EXPERIMENTAL MODEL AND SUBJECT DETAILS
  - Animals
  - Primary cell cultures
- METHOD DETAILS
  - Study design
  - Induction of brain ischemia
  - Drug treatments
  - Induction of Parabiosis
  - Generation of chimeric mice
  - Brain tissue processing and Flow cytometry
  - Cell isolation
  - Antigen-specific T cell proliferation assay
  - Immunofluorescence
  - RNA Extraction
  - RT-PCR
  - Transcriptomic analysis
  - ImmGen transcriptomic data comparison
  - Enrichment analysis
  - Quantification of middle cerebral artery anastomoses
- QUANTIFICATION AND STATISTICAL ANALYSIS

SUPPLEMENTAL INFORMATION

Supplemental Information can be found online at https://doi.org/10.1016/j.celrep.2020.108291.

ACKNOWLEDGMENTS

This work was funded by Ministerio de Ciencia, Innovación y Universidades (MICINN) co-financed by Fondo Europeo de Desarrollo Regional (FEDER) (SAF2017-87459-R), the European Union (EU) (H2020-ITN-2018-813294-ENTRAIN), and Fundació Marató TV3 (201723 to A.M.P. and D.S.). Work in the D.S. laboratory is funded by Centro Nacional de Investigaciones Cardiovasculares (CNIC), the European Research Council (ERC-2016-Consolidator Grant 725091), the EU (635122-PROCROP H2020), and MICINN-FEDER (SAF2016-79040-R). The EU (FP7-PEOPLE-2013-ITN-n°07962) supported M. Gallizioli. The PERIS program of Generalitat de Catalunya supported F.M.-M. A.O.-d.-A. had a fellowship from MICINN-FPI (BES-2015-074419). C.d.F. is supported by the AECC Foundation (INVES192DELF). We thank Anaxomics, the genomics and informatics BioCore Units of Centre for Genomic Regulation, the Cytomics and Experimental 7T MRI platforms of IDIBAPS, and the Advanced Optical Microscopy Unit-CCiT of the University of Barcelona for technical support. We thank Dr. U. Perpiñá for microscopy assistance. Plexxikon Inc. provided PLX5622 under a materials transfer agreement. Part of this work was performed at Centre de Recerca Biomèdica Cellex. The Centres de Recerca de Catalunya (CERCA) Program of Generalitat de Catalunya supports IDIBAPS.

AUTHOR CONTRIBUTIONS

Conceptualization, A.M.P., F.M.-M., D.S., C.d.F., M. Gelderblom, T.M., and M. Gallizioli; Methodology, F.M.-M., M. Gallizioli, M. Gelderblom, E.C., and C.J.; Formal Analysis, A.M.P., M. Gallizioli, and F.M.-M; Investigation, M. Gallizioli, F.M.-M., A.O.-d.-A., A.S.-P., R.C., C.J., V.H.B., F.R.-J., M.A.-R., J.P., and E.B.-T.; Resources, D.S. and C.d.F.; Writing – Original Draft, A.M.P.; Writing – Review & Editing: M. Gallizioli, A.M.P., F.M.-M., D.S., C.d.F., M. Gelderblom, E.C., and T.M.; Visualization, A.M.P., M. Gallizioli, and F.M.-M.; Supervision, A.M.P. and F.M.-M.; Project Administration, A.M.P.; Funding Acquisition, A.M.P., D.S., F.M.-M., and C.d.F.

DECLARATION OF INTERESTS

The authors declare no competing interests.

Received: May 4, 2020
Revised: September 2, 2020
Accepted: September 29, 2020
Published: October 20, 2020

REFERENCES

Amat, M., Benjamim, C.F., Williams, L.M., Prats, N., Terricabras, E., Beleta, J., Kunkel, S.L., and Godessart, N. (2006). Pharmacological blockade of CCR1 ameliorates murine arthritis and alters cytokine networks in vivo. Br. J. Pharmacol. *149*, 666–675.

Anandasabapathy, N., Victora, G.D., Meredith, M., Feder, R., Dong, B., Kluger, C., Yao, K., Dustin, M.L., Nussenzweig, M.C., Steinman, R.M., and Liu, K. (2011). Flt3L controls the development of radiosensitive dendritic cells in the meninges and choroid plexus of the steady-state mouse brain. J. Exp. Med. *208*, 1695–1705.

Arnold, I.C., Zhang, X., Artola-Boran, M., Fallegger, A., Sander, P., Johansen, P., and Müller, A. (2019). BATF3-dependent dendritic cells drive both effector and regulatory T-cell responses in bacterially infected tissues. PLoS Pathog. *15*, e1007866.

Ashburner, M., Ball, C.A., Blake, J.A., Botstein, D., Butler, H., Cherry, J.M., Davis, A.P., Dolinski, K., Dwight, S.S., Eppig, J.T., et al.; The Gene Ontology Consortium (2000). Gene Ontology: tool for the unification of biology. Nat. Genet. *25*, 25–29.

Benmamar-Badel, A., Owens, T., and Wlodarczyk, A. (2020). Protective microglial subset in development, aging, and disease: lessons from transcriptomic studies. Front. Immunol. *11*, 430.

Bonfill-Teixidor, E., Otxoa-de-Amezaga, A., Font-Nieves, M., Sans-Fons, M.G., and Planas, A.M. (2017). Differential expression of E-type prostanoid receptors 2 and 4 in microglia stimulated with lipopolysaccharide. J. Neuroinflammation *14*, 3.

Bourque, J., and Hawiger, D. (2018). immunomodulatory bonds of the partnership between dendritic cells and T cells. Crit. Rev. Immunol. *38*, 379–401.

Bulloch, K., Miller, M.M., Gal-Toth, J., Milner, T.A., Gottfried-Blackmore, A., Waters, E.M., Kaunzner, U.W., Liu, K., Lindquist, R., Nussenzweig, M.C., et al. (2008). CD11c/EYFP transgene illuminates a discrete network of dendritic cells within the embryonic, neonatal, adult, and injured mouse brain. J. Comp. Neurol. *508*, 687–710.

Butovsky, O., Bukshpan, S., Kunis, G., Jung, S., and Schwartz, M. (2007). Microglia can be induced by IFN-gamma or IL-4 to express neural or dendritic-like markers. Mol. Cell. Neurosci. *35*, 490–500.

Chamorro, Á., Meisel, A., Planas, A.M., Urra, X., van de Beek, D., and Veltkamp, R. (2012). The immunology of acute stroke. Nat. Rev. Neurol. *8*, 401–410.

Chamorro, Á., Dirnagl, U., Urra, X., and Planas, A.M. (2016). Neuroprotection in acute stroke: targeting excitotoxicity, oxidative and nitrosative stress, and inflammation. Lancet Neurol. *15*, 869–881.

Clarkson, B.D., Héninger, E., Harris, M.G., Lee, J., Sandor, M., and Fabry, Z. (2012). Innate-adaptive crosstalk: how dendritic cells shape immune responses in the CNS. Adv. Exp. Med. Biol. *946*, 309–333.

Coates, P.T.H., Barratt-Boyes, S.M., Zhang, L., Donnenberg, V.S., O'Connell, P.J., Logar, A.J., Duncan, F.J., Murphey-Corb, M., Donnenberg, A.D., Morelli, A.E., et al. (2003). Dendritic cell subsets in blood and lymphoid tissue of rhesus monkeys and their mobilization with Flt3 ligand. Blood *102*, 2513–2521.

Coombes, J.L., Siddiqui, K.R., Arancibia-Cárcamo, C.V., Hall, J., Sun, C.M., Belkaid, Y., and Powrie, F. (2007). A functionally specialized population of mucosal CD103+ DCs induces Foxp3+ regulatory T cells via a TGF-beta and retinoic acid-dependent mechanism. J. Exp. Med. *204*, 1757–1764.

Croft, M., So, T., Duan, W., and Soroosh, P. (2009). The significance of OX40 and OX40L to T-cell biology and immune disease. Immunol. Rev. *229*, 173–191.

D'Agostino, P.M., Gottfried-Blackmore, A., Anandasabapathy, N., and Bulloch, K. (2012). Brain dendritic cells: biology and pathology. Acta Neuropathol. *124*, 599–614.

Dando, S.J., Naranjo Golborne, C., Chinnery, H.R., Ruitenberg, M.J., and McMenamin, P.G. (2016). A case of mistaken identity: CD11c-eYFP(+) cells in the normal mouse brain parenchyma and neural retina display the phenotype of microglia, not dendritic cells. Glia *64*, 1331–1349.

Del Fresno, C., and Sancho, D. (2019). cDC1s: new orchestrators of tissue innate immunity. Trends Immunol. *40*, 559–561.

del Fresno, C., Saz-Leal, P., Enamorado, M., Wculek, S.K., Martínez-Cano, S., Blanco-Menéndez, N., Schulz, O., Gallizioli, M., Miró-Mur, F., Cano, E., et al. (2018). DNGR-1 in dendritic cells limits tissue damage by dampening neutrophil recruitment. Science *362*, 351–356.

Dirnagl, U., Iadecola, C., and Moskowitz, M.A. (1999). Pathobiology of ischaemic stroke: an integrated view. Trends Neurosci. *22*, 391–397.

Domínguez, P.M., and Ardavín, C. (2010). Differentiation and function of mouse monocyte-derived dendritic cells in steady state and inflammation. Immunol. Rev. *234*, 90–104.

Enamorado, M., Iborra, S., Priego, E., Cueto, F.J., Quintana, J.A., Martínez-Cano, S., Mejías-Pérez, E., Esteban, M., Melero, I., Hidalgo, A., and Sancho, D. (2017). Enhanced anti-tumour immunity requires the interplay between resident and circulating memory CD8$^+$ T cells. Nat. Commun. *8*, 16073.

Felger, J.C., Abe, T., Kaunzner, U.W., Gottfried-Blackmore, A., Gal-Toth, J., McEwen, B.S., Iadecola, C., and Bulloch, K. (2010). Brain dendritic cells in ischemic stroke: time course, activation state, and origin. Brain Behav. Immun. *24*, 724–737.

Ford, A.L., Goodsall, A.L., Hickey, W.F., and Sedgwick, J.D. (1995). Normal adult ramified microglia separated from other central nervous system macrophages by flow cytometric sorting. Phenotypic differences defined and direct ex vivo antigen presentation to myelin basic protein-reactive CD4+ T cells compared. J. Immunol. *154*, 4309–4321.

Frolkis, A., Knox, C., Lim, E., Jewison, T., Law, V., Hau, D.D., Liu, P., Gautam, B., Ly, S., Guo, A.C., et al. (2010). SMPDB: The Small Molecule Pathway Database. Nucleic Acids Res. *38*, D480–D487.

Gelderblom, M., Gallizioli, M., Ludewig, P., Thom, V., Arunachalam, P., Rissiek, B., Bernreuther, C., Glatzel, M., Korn, T., Arumugam, T.V., et al. (2018). IL-23 (interleukin-23)-producing conventional dendritic cells control the detrimental IL-17 (interleukin-17) response in stroke. Stroke *49*, 155–164.

Gong, T., Liu, L., Jiang, W., and Zhou, R. (2020). DAMP-sensing receptors in sterile inflammation and inflammatory diseases. Nat. Rev. Immunol. *20*, 95–112.

Greter, M., Heppner, F.L., Lemos, M.P., Odermatt, B.M., Goebels, N., Laufer, T., Noelle, R.J., and Becher, B. (2005). Dendritic cells permit immune invasion of the CNS in an animal model of multiple sclerosis. Nat. Med. *11*, 328–334.

Guermonprez, P., Helft, J., Claser, C., Deroubaix, S., Karanje, H., Gazumyan, A., Darasse-Jèze, G., Telerman, S.B., Breton, G., Schreiber, H.A., et al. (2013). Inflammatory Flt3l is essential to mobilize dendritic cells and for T cell responses during Plasmodium infection. Nat. Med. *19*, 730–738.

Guilliams, M., Ginhoux, F., Jakubzick, C., Naik, S.H., Onai, N., Schraml, B.U., Segura, E., Tussiwand, R., and Yona, S. (2014). Dendritic cells, monocytes and macrophages: a unified nomenclature based on ontogeny. Nat. Rev. Immunol. *14*, 571–578.

Hatano, R., Ohnuma, K., Otsuka, H., Komiya, E., Taki, I., Iwata, S., Dang, N.H., Okumura, K., and Morimoto, C. (2015). CD26-mediated induction of EGR2 and IL-10 as potential regulatory mechanism for CD26 costimulatory pathway. J. Immunol. *194*, 960–972.

Hildner, K., Edelson, B.T., Purtha, W.E., Diamond, M., Matsushita, H., Kohyama, M., Calderon, B., Schraml, B.U., Unanue, E.R., Diamond, M.S., et al. (2008). Batf3 deficiency reveals a critical role for CD8alpha+ dendritic cells in cytotoxic T cell immunity. Science *322*, 1097–1100.

Huang, W., Sherman, B.T., and Lempicki, R.A. (2009). Systematic and integrative analysis of large gene lists using DAVID bioinformatics resources. Nat. Protoc. *4*, 44–57.

Iadecola, C., and Alexander, M. (2001). Cerebral ischemia and inflammation. Curr. Opin. Neurol. *14*, 89–94.

Iadecola, C., and Anrather, J. (2011). The immunology of stroke: from mechanisms to translation. Nat. Med. *17*, 796–808.

ImmGen Consortium (2016). Open-source ImmGen: mononuclear phagocytes. Nat. Immunol. *17*, 741.

Jacquemin, C., Augusto, J.-F., Scherlinger, M., Gensous, N., Forcade, E., Douchet, I., Levionnois, E., Richez, C., Lazaro, E., Duffau, P., et al. (2018). OX40L/OX40 axis impairs follicular and natural Treg function in human SLE. JCI Insight *3*, e122167.

Janela, B., Patel, A.A., Lau, M.C., Goh, C.C., Msallam, R., Kong, W.T., Fehlings, M., Hubert, S., Lum, J., Simoni, Y., et al. (2019). A subset of type I conventional dendritic cells controls cutaneous bacterial infections through VEGFα-mediated recruitment of neutrophils. Immunity *50*, 1069–1083.e8.

Jiang, H., Lei, R., Ding, S.-W., and Zhu, S. (2014). Skewer: a fast and accurate adapter trimmer for next-generation sequencing paired-end reads. BMC Bioinformatics *15*, 182.

Jorba, G., Aguirre-Plans, J., Junet, V., Segú-Vergés, C., Ruiz, J.L., Pujol, A., Fernández-Fuentes, N., Mas, J.M., and Oliva, B. (2020). In-silico simulated prototype-patients using TPMS technology to study a potential adverse effect of sacubitril and valsartan. PLoS ONE *15*, e0228926.

Kamphuis, W., Kooijman, L., Schetters, S., Orre, M., and Hol, E.M. (2016). Transcriptional profiling of CD11c-positive microglia accumulating around amyloid plaques in a mouse model for Alzheimer's disease. Biochim. Biophys. Acta *1862*, 1847–1860.

Kanehisa, M., Furumichi, M., Tanabe, M., Sato, Y., and Morishima, K. (2017). KEGG: new perspectives on genomes, pathways, diseases and drugs. Nucleic Acids Res. *45* (*D1*), D353–D361.

Kaunzner, U.W., Miller, M.M., Gottfried-Blackmore, A., Gal-Toth, J., Felger, J.C., McEwen, B.S., and Bulloch, K. (2012). Accumulation of resident and peripheral dendritic cells in the aging CNS. Neurobiol. Aging *33*, 681–693.e1.

Khare, A., Krishnamoorthy, N., Oriss, T.B., Fei, M., Ray, P., and Ray, A. (2013). Cutting edge: inhaled antigen upregulates retinaldehyde dehydrogenase in lung CD103$^+$ but not plasmacytoid dendritic cells to induce Foxp3 de novo in CD4$^+$ T cells and promote airway tolerance. J. Immunol. *191*, 25–29.

Kierdorf, K., Katzmarski, N., Haas, C.A., and Prinz, M. (2013). Bone marrow cell recruitment to the brain in the absence of irradiation or parabiosis bias. PLoS ONE *8*, e58544.

Kostulas, N., Li, H.-L., Xiao, B.-G., Huang, Y.-M., Kostulas, V., and Link, H. (2002). Dendritic cells are present in ischemic brain after permanent middle cerebral artery occlusion in the rat. Stroke *33*, 1129–1134.

Li, Y., Song, Y., Zhao, L., Gaidosh, G., Laties, A.M., and Wen, R. (2008). Direct labeling and visualization of blood vessels with lipophilic carbocyanine dye DiI. Nat. Protoc. *3*, 1703–1708.

Liesz, A., Suri-Payer, E., Veltkamp, C., Doerr, H., Sommer, C., Rivest, S., Giese, T., and Veltkamp, R. (2009). Regulatory T cells are key cerebroprotective immunomodulators in acute experimental stroke. Nat. Med. *15*, 192–199.

Lipfert, J., Ödemis, V., Wagner, D.-C., Boltze, J., and Engele, J. (2013). CXCR4 and CXCR7 form a functional receptor unit for SDF-1/CXCL12 in primary rodent microglia. Neuropathol. Appl. Neurobiol. *39*, 667–680.

Love, M.I., Huber, W., and Anders, S. (2014). Moderated estimation of fold change and dispersion for RNA-seq data with DESeq2. Genome Biol. *15*, 550.

Ludewig, P., Gallizioli, M., Urra, X., Behr, S., Brait, V.H., Gelderblom, M., Magnus, T., and Planas, A.M. (2016). Dendritic cells in brain diseases. Biochim. Biophys. Acta *1862*, 352–367.

Lysenko, O., Schulte, D., Mittelbronn, M., and Steinle, A. (2013). BACL is a novel brain-associated, non-NKC-encoded mammalian C-type lectin-like receptor of the CLEC2 family. PLoS ONE *8*, e65345.

Malo, C.S., Huggins, M.A., Goddery, E.N., Tolcher, H.M.A., Renner, D.N., Jin, F., Hansen, M.J., Pease, L.R., Pavelko, K.D., and Johnson, A.J. (2018). Non-equivalent antigen presenting capabilities of dendritic cells and macrophages in generating brain-infiltrating CD8$^+$ T cell responses. Nat. Commun. *9*, 633.

Miller, J.C., Brown, B.D., Shay, T., Gautier, E.L., Jojic, V., Cohain, A., Pandey, G., Leboeuf, M., Elpek, K.G., Helft, J., et al.; Immunological Genome Consortium (2012). Deciphering the transcriptional network of the dendritic cell lineage. Nat. Immunol. *13*, 888–899.

Mohammad, M.G., Tsai, V.W.W., Ruitenberg, M.J., Hassanpour, M., Li, H., Hart, P.H., Breit, S.N., Sawchenko, P.E., and Brown, D.A. (2014). Immune cell trafficking from the brain maintains CNS immune tolerance. J. Clin. Invest. *124*, 1228–1241.

Mundt, S., Mrdjen, D., Utz, S.G., Greter, M., Schreiner, B., and Becher, B. (2019). Conventional DCs sample and present myelin antigens in the healthy CNS and allow parenchymal T cell entry to initiate neuroinflammation. Sci. Immunol. *4*, eaau8380.

Ohnuma, K., Dang, N.H., and Morimoto, C. (2008). Revisiting an old acquaintance: CD26 and its molecular mechanisms in T cell function. Trends Immunol. *29*, 295–301.

Otxoa-de-Amezaga, A., Miró-Mur, F., Pedragosa, J., Gallizioli, M., Justicia, C., Gaja-Capdevila, N., Ruíz-Jaen, F., Salas-Perdomo, A., Bosch, A., Calvo, M., et al. (2019). Microglial cell loss after ischemic stroke favors brain neutrophil accumulation. Acta Neuropathol. *137*, 321–341.

Poczobutt, J.M., De, S., Yadav, V.K., Nguyen, T.T., Li, H., Sippel, T.R., Weiser-Evans, M.C.M., and Nemenoff, R.A. (2016). Expression profiling of macrophages reveals multiple populations with distinct biological roles in an immunocompetent orthotopic model of lung cancer. J. Immunol. *196*, 2847–2859.

Prodinger, C., Bunse, J., Krüger, M., Schiefenhövel, F., Brandt, C., Laman, J.D., Greter, M., Immig, K., Heppner, F., Becher, B., and Bechmann, I. (2011). CD11c-expressing cells reside in the juxtavascular parenchyma and extend processes into the glia limitans of the mouse nervous system. Acta Neuropathol. *121*, 445–458.

Quintana, E., Fernández, A., Velasco, P., de Andrés, B., Liste, I., Sancho, D., Gaspar, M.L., and Cano, E. (2015). DNGR-1(+) dendritic cells are located in meningeal membrane and choroid plexus of the noninjured brain. Glia *63*, 2231–2248.

Ransohoff, R.M., and Engelhardt, B. (2012). The anatomical and cellular basis of immune surveillance in the central nervous system. Nat. Rev. Immunol. *12*, 623–635.

Reichmann, G., Schroeter, M., Jander, S., and Fischer, H.-G. (2002). Dendritic cells and dendritic-like microglia in focal cortical ischemia of the mouse brain. J. Neuroimmunol. *129*, 125–132.

Rivals, I., Personnaz, L., Taing, L., and Potier, M.-C. (2007). Enrichment or depletion of a GO category within a class of genes: which test? Bioinformatics *23*, 401–407.

Salas-Perdomo, A., Miró-Mur, F., Urra, X., Justicia, C., Gallizioli, M., Zhao, Y., Brait, V.H., Laredo, C., Tudela, R., Hidalgo, A., et al. (2018). T cells prevent hemorrhagic transformation in ischemic stroke by P-selectin binding. Arterioscler. Thromb. Vasc. Biol. *38*, 1761–1771.

Sancho, D., Joffre, O.P., Keller, A.M., Rogers, N.C., Martínez, D., Hernanz-Falcón, P., Rosewell, I., and Reis e Sousa, C. (2009). Identification of a dendritic cell receptor that couples sensing of necrosis to immunity. Nature *458*, 899–903.

Schlitzer, A., McGovern, N., and Ginhoux, F. (2015). Dendritic cells and monocyte-derived cells: Two complementary and integrated functional systems. Semin. Cell Dev. Biol. *41*, 9–22.

Schraml, B.U., van Blijswijk, J., Zelenay, S., Whitney, P.G., Filby, A., Acton, S.E., Rogers, N.C., Moncaut, N., Carvajal, J.J., and Reis e Sousa, C. (2013). Genetic tracing via DNGR-1 expression history defines dendritic cells as a hematopoietic lineage. Cell *154*, 843–858.

Shannon, P., Markiel, A., Ozier, O., Baliga, N.S., Wang, J.T., Ramage, D., Amin, N., Schwikowski, B., and Ideker, T. (2003). Cytoscape: a software environment for integrated models of biomolecular interaction networks. Genome Res. *13*, 2498–2504.

Silvin, A., and Ginhoux, F. (2018). Microglia heterogeneity along a spatio-temporal axis: More questions than answers. Glia *66*, 2045–2057.

Subramanian, A., Tamayo, P., Mootha, V.K., Mukherjee, S., Ebert, B.L., Gillette, M.A., Paulovich, A., Pomeroy, S.L., Golub, T.R., Lander, E.S., and Mesirov, J.P. (2005). Gene set enrichment analysis: a knowledge-based approach for interpreting genome-wide expression profiles. Proc. Natl. Acad. Sci. U S A *102*, 15545–15550.

Sun, C.M., Hall, J.A., Blank, R.B., Bouladoux, N., Oukka, M., Mora, J.R., and Belkaid, Y. (2007). Small intestine lamina propria dendritic cells promote de

novo generation of Foxp3 T reg cells via retinoic acid. J. Exp. Med. *204*, 1775–1785.

The UniProt Consortium (2017). UniProt: the universal protein knowledgebase. Nucleic Acids Res. *45* (*D1*), D158–D169.

Torres, M., Rojas, M., Campillo, N., Cardenes, N., Montserrat, J.M., Navajas, D., and Farré, R. (2015). Parabiotic model for differentiating local and systemic effects of continuous and intermittent hypoxia. J. Appl. Physiol. *118*, 42–47.

Toubai, T., Malter, C., Tawara, I., Liu, C., Nieves, E., Lowler, K.P., Sun, Y., and Reddy, P. (2010). Immunization with host-type CD8alpha+ dendritic cells reduces experimental acute GVHD in an IL-10-dependent manner. Blood *115*, 724–735.

Whirl-Carrillo, M., McDonagh, E.M., Hebert, J.M., Gong, L., Sangkuhl, K., Thorn, C.F., Altman, R.B., and Klein, T.E. (2012). Pharmacogenomics knowledge for personalized medicine. Clin. Pharmacol. Ther. *92*, 414–417.

Wlodarczyk, A., Løbner, M., Cédile, O., and Owens, T. (2014). Comparison of microglia and infiltrating CD11c^{+} cells as antigen presenting cells for T cell proliferation and cytokine response. J. Neuroinflammation *11*, 57.

Wlodarczyk, A., Holtman, I.R., Krueger, M., Yogev, N., Bruttger, J., Khorooshi, R., Benmamar-Badel, A., de Boer-Bergsma, J.J., Martin, N.A., Karram, K., et al. (2017). A novel microglial subset plays a key role in myelinogenesis in developing brain. EMBO J. *36*, 3292–3308.

STAR★METHODS

KEY RESOURCES TABLE

REAGENT or RESOURCE	SOURCE	IDENTIFIER
Antibodies		
Anti-mouse CD11b (clone M1/70, APC-Cy7	BD Biosciences	557657; RRID:AB_396772
Anti-mouse CD11b (clone M1/70, BV605)	BioLegend	101237; RRID:AB_11126744
Anti-mouse CD45 (clone 30-F11, BV786)	BD Biosciences	564225; RRID:AB_2716861
Anti-mouse CD45 (clone 30-F11 APC-eFluor780)	Thermo Fisher Scientific	47-0451-82; RRID:AB_1548781
Anti-mouse Ly6G (clone 1A8, PE-Cy7)	BD Biosciences	560601; RRID:AB_1727562
Anti-mouse Ly6G (clone 1A8, Alexa Fluor 700)	BioLegend	127621; RRID:AB_10640452
Anti-mouse F4/80 (clone BM8, BV605)	BioLegend	123133; RRID:AB_2562305
Anti-mouse Ly6C (clone HK1.4, eFluor 450) or	Thermo Fisher Scientific	48-5932-82; RRID:AB_10805519
Anti-mouse Ly6C (clone HK1.4, PerCP/Cy5.5)	BioLegend	128011; RRID:AB_1659242
Anti-mouse XCR1 (clone ZET, BV421)	BioLegend	148216; RRID:AB_2565230
Anti-mouse CD103 (clone M290, BV711)	BD Biosciences	564320; RRID:AB_2738743
Anti-mouse B220 (clone RA3-6B2, BV785)	BioLegend	103245; RRID:AB_11218795
Anti-mouse MHCII (I-A/I-E, clone M5/114.15.2, FITC)	Thermo Fisher Scientific	11-5321-82; RRID:AB_465232
Anti-mouse MHCII (I-A/I-E,clone M5/114.15.2, BV711)	BioLegend	107643; RRID:AB_2565976
Anti-mouse CD172a (clone P84, PE)	BD Biosciences	560107; RRID:AB_1645248
Anti-mouse CD64 (clone X54-5/7.1, PE-Cy7)	BioLegend	139313; RRID:AB_2563903
Anti-mouse CD11c (clone N418, APC)	Thermo Fisher Scientific	17-0114-82; RRID:AB_469346
Anti-mouse CD11c (clone N418, FITC)	Bio-Rad	MCA1369F; RRID:AB_324141
Anti-mouse CD31 (clone 390, PE-Cy7)	Thermo Fisher Scientific	25-0311-82; RRID:AB_2716949
Anti-mouse CD45 (clone 30-F11, FITC)	BD Biosciences	561088; RRID:AB_10562038
Anti-mouse CD11b (clone M1/70, Alexa Fluor 647)	BD Biosciences	557686; RRID:AB_396796
Anti-Mouse CD16/CD32 (Mouse BD Fc Block, Clone 2.4G2)	BD Biosciences	553142; RRID:AB_394657
Anti-Mouse ACSA2 (Clone IH3-18A3, PE)	Miltenyi Biotec	130-102-365; RRID:AB_2651189
Rabbit polyclonal anti-mouse laminin	Agilent	Z0097; RRID:AB_2313665
Anti-mouse P2RY12	AnaSpec	55043A; RRIB:AB_2298886
Anti-mouse Iba1	Wako Chemicals	016-20001; RRID:AB_839506
Anti-mouse Myelin Basic Protein [BDI221]	Abcam	ab66188; RRID:AB_1141067
Chemicals, Peptides, and Recombinant Proteins		
PLX5622	Plexxikon Inc.	N/A
Recombinant Murine Flt3-Ligand	Peprotech	250-31L
Collagenase from Clostridium histolyticum	Sigma Aldrich	C5138
Deoxyribonuclease I from bovine pancreas	Sigma Aldrich	D5025-150KU
Percoll®	GE Healthcare	17-0891-01
HBSS, no calcium, no magnesium, no phenol red	Thermo Fisher Scientific	14175-053
LIVE/DEAD Fixable Aqua Dead Cell Stain Kit, for 405 nm excitation	Thermo Fisher Scientific	L34957
HBSS, calcium, magnesium, no phenol red	Thermo Fisher Scientific	14025-092
Stain Buffer (FBS)	BD Biosciences	554656
Neural Tissue Dissociation Kit (P)	Miltenyi Biotec	130-092-628
Myelin Removal Beads II	Miltenyi Biotec	130-096-433
DPBS no calcium, no magnesium	Thermo Fisher Scientific	14190-094

(*Continued on next page*)

Continued

REAGENT or RESOURCE	SOURCE	IDENTIFIER
Adult Brain Tissue Dissociation Kit	Miltenyi Biotec	130-107-677
Debris Removal Solution	Miltenyi Biotec	130-109-398
Red Blood Cell Removal Solution	Miltenyi Biotec	130-094-183
Anti-ACSA-2 microbead kit, mouse	Miltenyi Biotec	130-097-678
AstroMACS Separation Buffer	Miltenyi Biotec	130-117-336
Pan T Cell Isolation Kit II	Miltenyi Biotec	130-095-130
CellTrace Violet Cell Proliferation Kit	Invitrogen	C34557
Recombinant murine IL-2	Peprotech	212-12
Ovalbumin (323-339) (chicken, Japanese quail)	Sigma Aldrich	O1641
Ovalbumin (257-264) (chicken) SIINFEKL	Sigma Aldrich	S7951
Recombinant Murine IL-4	Peprotech	214-14
Lipopolysaccharides from *Escherichia coli* O55:B5	Sigma Aldrich	L2880
TO-PRO-3 Iodide (642/661)	Thermo Fisher Scientific	T3605
High Capacity cDNA Reverse Transcription kit	Applied Biosystems	4387406
TaqMan® Pre Amp Master Mix (2 ×)	Thermo Fisher Scientific	4384266
TE Buffer, Tris-EDTA, 1X Solution, pH 8.0	Fisher Scientific	BP2473
TaqMan Universal PCR Master Mix	Thermo Fisher Scientific	4304437
TruSeq Stranded mRNA Sample Prep Kit v2	Illumina	RS-122-2101/2
SuperScript II reverse transcriptase	Invitrogen	18064-014
SMART-Seq v4 Ultra Low Input RNA kit	Clontech	634890
NEBNext Ultra DNA Library Prep kit	New England Biolabs	E7370
DiI (1,1′-Dioctadecyl-3,3,3′,3′-tetramethylindocarbocyanine perchlorate)	Sigma Aldrich	42364
Critical Commercial Assays		
KAPA Library Quantification Kit	KapaBiosystems	KK4835
Deposited Data		
RNA-Seq data	This paper	GEO: GSE136856
Experimental Models: Organisms/Strains		
Mouse: CD11c-eYFP; Tg(Itgax-Venus)1Mnz	The Jackson Laboratory	SN8829
Mouse: CX3CR1Cre^{ERT2}; B6.129P2(C)-Cx3cr1tm2.1 (cre/ERT2)Jung/J	The Jackson Laboratory	SN020940
Mouse: ROSA26-tdTomato; (B6.Cg-Gt(ROSA) 26Sortm9(CAG-tdTomato)Hze/J	The Jackson Laboratory	SN007909
Mouse: Rag1/OTI; B6.129S7-Rag1tm1Mom Tg(TcraTcrb)1100Mjb	Taconic	4175
Mouse: OTII; B6.Cg-Tg(TcraTcrb)425Cbn/J	The Jackson Laboratory	SN004194
Mouse: C57BL/6J	Janvier	SC-C57J-M
Oligonucleotides		
See Table S4		N/A
Software and Algorithms		
R software, DESEQ2 package	(Love, Huber, and Anders 2014)	https://bioconductor.org/packages/release/bioc/html/DESeq2.html
FacsDiva v5	BD Biosciences	https://www.bdbiosciences.com/en-us/instruments/research-instruments/research-software/flow-cytometry-acquisition/facsdiva-software
FlowJo v10	FlowJo LLC	https://www.flowjo.com/solutions/flowjo
FastQC v0.11.5	Babraham Bioinformatics	https://www.bioinformatics.babraham.ac.uk/projects/download.html#fastqc
Skewer (v0.2.2)	(Jiang et al., 2014)	http://bioweb.pasteur.fr/packages/pack@skewer@0.2.2

(*Continued on next page*)

Continued

REAGENT or RESOURCE	SOURCE	IDENTIFIER
Immgen 'Population Comparison tool'	(ImmGen Consortium 2016)	http://rstats.immgen.org/PopulationComparison/
Immgen 'My Gene Set tool'	(ImmGen Consortium 2016)	http://rstats.immgen.org/MyGeneSet_New/index.html
DAVID Bioinformatics Resources 6.7	(Huang, Sherman, and Lempicki 2009)	https://david.ncifcrf.gov/home.jsp
Cytoscape v3.5.1	(Shannon et al., 2003)	http://chianti.ucsd.edu/cytoscape-3.5.1/
Prism v.8	GraphPad	https://www.graphpad.com/scientific-software/prism/

RESOURCE AVAILABILITY

Lead Contact

Further information and requests for resources and reagents should be directed to and will be fulfilled by the Lead Contact, Anna M. Planas (anna.planas@iibb.csic.es).

Materials Availability

This study did not generate new unique reagents.

Data and Code Availability

The RNA-Seq data are accessible from the GEO repository of the National Center for Biotechnology Information, U.S. National Library of Medicine (The accession number for these data is GEO: GSE136856) (https://www.ncbi.nlm.nih.gov/geo/info/linking.html). Other datasets are available from the corresponding author upon reasonable request.

EXPERIMENTAL MODEL AND SUBJECT DETAILS

Animals

We used adult (3-4 month old) mice in the C57BL/6 background. We used CD11c-eYFP reporter mice (Tg(Itgax-Venus)1Mnz; #SN8829) that were maintained as hemizygous by crossing with C57BL/6 mice; CX3CR1cre^{ERT2} mice (B6.129P2(C)-Cx3cr1tm2.1(cre/ERT2)Jung/J, #SN020940) crossed with reporter ROSA26-tdTomato mice (B6.Cg-Gt(ROSA)26Sortm9(CAG-tdTomato)Hze/J, #SN007909) that received tamoxifen three weeks before surgery; and OTII mice (B6.Cg-Tg(TcraTcrb)425Cbn/J, #SN004194); all obtained from The Jackson Laboratory. Colonies of *Batf3*$^{-/-}$ mice and *Batf3*$^{+/+}$ wild-type mice (Enamorado et al., 2017) and OTI mice (OT-I transgenic mice – C57BL/6-Tg(TcraTcrb)11003Mjb/J, #003831 – crossed with Rag1$^{-/-}$ mice – B6.129S7-Rag1tm1Mom/J, #002216 – both from The Jackson Laboratories) were kept under SPF in the animal house of CNIC and were transferred to the animal house of the School of Medicine of UB for induction of ischemia. Additional C57BL/6 wild-type mice (#SC-C57J-M) were purchased from Janvier (France). Prior to experiments all mice were maintained under SPF conditions in the animal house of the School of Medicine of the University of Barcelona (UB). Unless otherwise stated we used male mice. Studies of parabiosis were carried out in female mice and corresponding non-parabiotic female mice were used for comparative purposes. We always compared mice of the same sex given that we did not investigate sex effects in this study. Animal work was conducted following the Catalan and Spanish laws (Real Decreto 53/2013) and the European Directives. All experiments were conducted with approval of the ethical committee (Comité Ètic d'Experimentació Animal, CEEA) of UB, and the local regulatory bodies of the Generalitat de Catalunya, and in compliance with the NIH Guide for the Care and Use of Laboratory Animals. The work is reported following the ARRIVE guidelines.

Primary cell cultures

We prepared primary glial cell cultures from the cerebral cortex of 1-to 2-day-old newborn C57BL/6 mice of both sexes as reported (Bonfill-Teixidor et al., 2017). In brief, we removed the meninges and dissociated the tissue with 0.025% trypsin containing 1mM EDTA (GIBCO) under shaking for 30 min at 37°C. We then added DMEM:F12 with 10% FBS (GIBCO) and 4mg/mL DNase (Sigma-Aldrich). After centrifugation at 300 x*g* for 5 min, cells were seeded in DMEM-F12 with 20% FBS and 1% penicillin/streptomycin (P/S) 10,000 U/10,000 μg/mL (GIBCO) at a density of 250,000 cells/mL in 25cm^2 tissue culture flasks. The cells were maintained at 37°C in a humidified atmosphere of 5% CO_2-95% air for 8 days. Cells were subcultured at 8 days *in vitro*. After two washes in PBS, cells were treated with 0.125% trypsin-EDTA for 5 min at 37°C. Neutralization with supplemented media (1:1) was carried out and cells were seeded at 80,000 cells/mL in DMEM-F12 with 20% FBS and 1% P/S in poly-D-lysine-coated tissue culture plates. At confluence, cells were treated with mouse recombinant IL-4 (50 ng/mL, #214-14, Peprotech) or LPS (10 ng/mL; *Escherichia coli* 055:B5,# L2880 Sigma-Aldrich) and the cells were obtained at different time points for RNA extraction.

METHOD DETAILS

Study design

Our main objective was to compare microglia versus dendritic cells in different experimental groups. Randomization and blinding was conducted for treatment administration when possible, as stated below. Cerebral blood flow (CBF) data were used as predefined criteria to exclude animals from the study.

Induction of brain ischemia

Cerebral ischemia was induced by transient (45-min) occlusion of the right middle cerebral artery (MCAo) with the intraluminal technique, as described (Salas-Perdomo et al., 2018). In brief, anesthesia was induced with 4% isoflurane in a mixture of 30% O_2 and 70% N_2O and it was maintained with 1%–1.5% isoflurane in the same mixture by the aid of a facial mask. A longitudinal cut was produced in the ventral middle line of the neck to expose and ligate the right common carotid artery (CCA). Next the submaxillary glands and the omohyoid and sternothyroid muscles were separated, exposing the carotid arteries. A monofilament (#701912PK5Re, Doccol Corporation, Sharon, MA) was introduced through the right external carotid artery up to the level where the MCA branches out. CBF was monitored with laser Doppler flowmetry (Perimed, AB, Järfälla, Sweden). After 45 min of arterial occlusion, the filament was cautiously removed, and the suture of the ipsilateral CCA was removed to allow reperfusion. Mice received analgesia (buprenorphine, 150 μl of a 0.015 mg/mL solution, via i.p.) and were kept on a thermal blanket for 1 hour after surgery. Cerebral blood flow (CBF) data were used as predefined criteria to exclude animals from the study as follows: (1) mice with incorrect surgery or surgical complication; (2) mice that did not show a drop in CBF greater than 75% from basal CBF values after introducing the filament in the middle cerebral artery , as it was considered that ischemia was not successfully induced; and (3) mice that did not show recovery in CBF of higher than 70% of the basal value as reperfusion did not reach an adequate level.

Drug treatments

For microglia depletion, mice received the CSF1R inhibitor PLX5622 (Plexxikon Inc, Berkeley USA) following previously reported protocols (Otxoa-de-Amezaga et al., 2019). The inhibitor was mixed into AIN-76A standard chow at 1200 ppm (Brogaarden, Denmark). Mice (8-week old) received the diet *ad libitum* for three weeks prior to induction of ischemia and the diet was maintained until the mice were killed.

Treatment controls received AIN-76A chow for the same period of time. Both diets were given in parallel in groups of 5 animals per cage. Researchers conducting ischemia and obtaining further data were not aware of the identity of the diet groups.

Flt3L (10 μg per mouse, #250-31L, Peprotech) was administered during 7 days using Alzet pumps (1007D, #0000290, Durect Corporation, USA) implanted subcutaneously. Ischemia was performed 3 days after pump implantation and mice were euthanized 4 days post-ischemia.

Daily injections of CCR1 antagonist J113863 (Tocris #2595, 10 mg/Kg dose, 300 μl/injection) were given i.p. starting 1 day post-ischemia and ending at day 3. Treatment controls received the same volume of the vehicle (phosphate buffer containing 10% Tween80). The dose of J113863 was decided following previous studies (Amat et al., 2006). Treatment was randomly assigned and was administered in a blinded fashion. The animals received a code that did not reveal the identity of the groups.

Induction of Parabiosis

We generated parabiotic pairs by joining 3-month old female CD11c-eYFP mice with wild-type female littermates, as reported (Torres et al., 2015). We obtained the brain tissue three weeks later. In some parabiotic pairs we induced ischemia in the wild-type mouse and the brain was obtained 4 days post-ischemia. For comparison purposes, we induced ischemia in non-parabiotic CD11c-eYFP and CX3CR1cre^{ert2}-ROSA26 tdT female mice.

Generation of chimeric mice

We generated chimeric mice by chemical ablation of the bone marrow of WT recipient mice followed by transplantation of bone marrow from either WT or *Batf3*$^{-/-}$ donor mice, as described (Kierdorf et al., 2013). In brief, adult (2-month old) male WT mice received three intraperitoneal injections of the chemotherapeutic agent busulfan (30 μg/g body weight) 7, 5 and 3 days prior to the transfer of five million bone marrow cells from Baft3$^{-/-}$ or WT donor mice via the tail vein. Ischemia was induced eight weeks after grafting.

Brain tissue processing and Flow cytometry

Mice were anesthetized and perfused transcardially with 30 mL PBS containing heparin (5 U/mL). The ischemic cortex (ipsilateral) and the corresponding region of the non-affected hemisphere (contralateral) were dissected and analyzed separately. The tissue was homogenized with gentleMACS Dissociator (#130-096-427, Miltenyi Biotec: 2x Brain_1 program and 1x ABDK_37C program by Miltenyi) while immersed in 2ml of HBSS buffer (w/o Ca^{2+} and Mg2+, #14175-053, Thermo Fisher Scientific) containing 100 U/mL collagenase IV (#C5138, Sigma) and 50 U/mL DNase I (#D5025-150 KU, Sigma). The tissue was then filtered on a cell strainer (70um) and the cells were separated from myelin and debris with a 30% percoll gradient (#17-0891-01, GE Healthcare) in HBSS without Ca^{2+} and Mg2+ centrifuged at 950 g during 20min without brakes. Cells were collected from the bottom of the

tube after centrifugation and washed with FACS buffer (PBS, 2 mM EDTA, 2% FBS). Unspecific binding of antibodies was blocked by previous incubation for 10 min with anti CD16/CD32 (Fc block, clone 2.4G2, BD PharMingen) in FACS buffer at 4°C. Live/dead Aqua cell stain (Thermo Fisher Scientific #L34957) was used to determine the viability of cells. Cells were incubated with the following primary antibodies during 20 minutes at 4°C: CD11b (clone M1/70, APC-Cy7, BD PharMingen #557657 or clone M1/70, Brilliant Violet 605, Biolegend #101237), CD45 (clone 30-F11, Brilliant Violet 786,BD Horizon #564225 or clone 30-F11 APC-eFluor780, eBioscience #47-0451-82), Ly6G (clone 1A8, PE-Cy7, BD Biosciences #560601 or clone 1A8, Alexa Fluor 700, Biolegend #127621), Ly6C (clone HK1.4, eFluor 450, eBioScience #48-5932-82 or clone HK1.4, PerCP/Cy5.5, Biolegend #128011), XCR1 (clone ZET, Brilliant Violet 421, Biolegend #148216), CD103 (clone M290, Brilliant Violet 711, BD Biosciences #564320), B220 (clone RA3-6B2, Brilliant Violet 785, Biolegend #103245), MHCII (clone M5/114.15.2, FITC, eBioscience #11-5321-82 or clone M5/114.15.2, Brilliant Violet 711, Biolegend #107643), CD172a (clone P84, PE, BD Biosciences #560107), CD64 (clone X54-5/7.1, PE-Cy7, Biolegend #139313), CD11c (clone N418, APC, eBioscience #17-0114-82 or clone N418, FITC, Bio-Rad #MCA1369F). Data was acquired in a BD LSRII cytometer using FacsDiva software (version 5, BD Biosciences, San Jose, CA, USA). Flow-Count Fluorospheres (Beckman-Coulter # 7547053) were used for absolute quantification. Data analyses were performed with FlowJo software (version 10, FlowJo LLC, Ashland, OR, USA).

Cell isolation

Myeloid cells, astrocytes, and endothelial cells were isolated from the brain of adult mice (13-14 weeks old) using different animals and procedures for each cell type. CD11c-eYFP^{+} cells and microglia were isolated from the brain of CD11c-eYFP mice or CX3CR1cre^{ERT2}-ROSA26 tdT mice respectively using Fluorescence Activated Cell Sorting (FACS). Brains were collected in cold HBSS buffer (w/o Ca^{2+} and $Mg^{2+,}$ #14175-053, Thermo Fisher Scientific). The brain tissue was enzymatically dissociated using the Neural Tissue Dissociation Kit (P) (#130-092-628, Miltenyi Biotec). The gentleMACS Dissociator (#130-096-427, Miltenyi Biotec) was used for mechanical dissociation steps following the Neural Tissue Dissociation Kit (P) protocol for dissociation without heaters. The digested tissue was filtered twice with 70 μm and 40 μm filters washing with HBSS (with Ca^{2+} and Mg^{2+}, #14025-092, Thermo Fisher Scientific). Cells were separated from myelin and debris by 30% isotonic percoll gradient (#17-0891-01, GE Healthcare) in Myelin Gradient Buffer (MGB). Samples were centrifuged at 950 xg for 30 min without acceleration or brake. Cells were collected from the bottom of the tube, washed once with FACS Stain Buffer (#554656, BD Biosciences), and processed for FACS (no staining required) in a FACSAriaII sorter (BD Biosciences).

Endothelial cells were isolated from the brain of adult wild-type mice by FACS. Brains were collected in cold HBSS buffer (w/o Ca^{2+} and Mg^{2+}). The brain tissue was enzymatically dissociated using the Neural Tissue Dissociation Kit (P) (#130-092-628, Miltenyi Biotec) and mechanical dissociation was carried out with the gentleMACS Dissociator. The digested tissue was filtered in 70 μm filters washing with HBSS (with Ca^{2+} and Mg^{2+}). Cells were separated from myelin by magnetic separation using Myelin Removal Beads II (#130-096-433, Miltenyi Biotec) and LS Columns according to manufacturer's instructions. Cells were resuspended in FACS buffer (PBS, 2 mM EDTA, 2% FBS). Fc receptors were blocked by previous incubation for 10 min with CD16/CD32 (clone 2.4G2, BD PharMingen) in FACS buffer at 4°C. Live/dead Aqua cell stain (#L34957, Invitrogen) was used to determine cell viability. Cells were incubated with the following primary antibodies: CD31 (# 25-0311-82, clone 390, PE-Cy7, BD Biosciences), CD45 (#561088, clone 30-F11, FITC, BD Biosciences), CD11b (#557686, clone M1/70, Alexa Fluor 647, BD Biosciences), and cells processed for FACS in a FACSAriaII sorter (BD Biosciences).

Astrocytes were isolated from the brain of adult wild-type mice (13-14 weeks old) using immunomagnetic separation (Miltenyi Biotec, Germany). Brains were collected in cold D-PBS buffer (#14190-094, Thermo Fisher Scientific). The brain tissue was enzymatically dissociated using the Adult Brain Tissue Dissociation Kit (#130-107-677, Miltenyi Biotec). The gentleMACS Dissociator was used for mechanical dissociation steps during 30 min at 37°C (program 37C_ABDK_01). The digested tissue was filtered (70 μm) with D-PBS. Myelin and cell debris are removed using the Debris Removal Solution (#130-109-398, Miltenyi Biotec) followed by removal of erythrocytes using the Red Blood Cell Removal Solution (#130-094-183, Miltenyi Biotec). Then, cells were magnetically labeled with Anti-ACSA-2 microbeads (#130-097-678, Miltenyi Biotec) diluted in AstroMACS Separation Buffer (#130-117-336, Miltenyi Biotec) for 15 min in the dark in the refrigerator (2–8°C). ACSA-2+ cells were collected using magnetic field columns. Cell purity was assessed by using the Anti-ACSA-2-PE clone IH3-18A3 (#130-102-365, Miltenyi Biotec).

Antigen-specific T cell proliferation assay

CD11c-eYFP^{+} cells and microglia were obtained from the ischemic brain tissue (day 4) and isolated as described above. Cells were resuspended in FACS buffer (PBS, 2 mM EDTA, 2% FBS). Fc receptors were blocked by previous incubation for 10 min with CD16/CD32 (clone 2.4G2, BD PharMingen) in FACS buffer at 4°C. Cells were incubated with the following primary antibodies: CD45 (clone 30-F11 APC-eFluor780, eBioscience #47-0451-82) and CD11b (#557686, clone M1/70, Alexa Fluor 647, BD Biosciences) and processed for FACS in a FACSAriaII sorter (BD Biosciences). For studies of class II antigen presentation, T cells were isolated from spleen of OTII mice by magnetic separation using Pan T Cell Isolation Kit II (#130-095-130, Miltenyi Biotec) according to manufacturer's instructions for manual cell separation with LS columns. T cells were stained with CellTrace Violet Cell Proliferation Kit (2 μM, #C34557, Invitrogen). Cells were co-cultured for 5 days at a 1:10 APC to T cell ratio in RPMI 1640 complete medium in the presence of recombinant murine IL-2 (10 ng/mL, #212-12, Peprotech) and OVA peptide 323-339 (2 μg/mL, #O1641, Sigma). The cells were washed with FACS buffer and data was acquired in a BD LSRII cytometer using FacsDiva software (version 5, BD Biosciences,

San Jose, CA, USA). The proliferation index is expressed as % of cells with reduction of the intensity of CellTrace Violet Staining. For studies of class I antigen presentation, CD8 T cells were isolated from the spleen of Rag1KO-OTI mice and stained with CellTrace Violet Cell Proliferation Kit as above. APCs were pulsed during 1h with SIINFEKL peptide (0.1 ng/mL, #S7951, Sigma) in RPMI 1640 complete medium and then extensively washed with RPMI 1640 complete medium. T Cells and peptide-pulsed APCs were co-cultured for 3 days at a 1:6 APC to T cell ratio in RPMI 1640 complete medium. After washing with FACS buffer, data was acquired in a BD LSRII cytometer using FacsDiva software (version 5, BD Biosciences, San Jose, CA, USA). The proliferation index is expressed as % of cells with reduction of the intensity of CellTrace Violet Staining.

Immunofluorescence

Mice were perfused through the heart with 40 mL of cold saline solution (0.9% NaCl) followed by 20 mL of cold 4% paraformaldehyde diluted in phosphate buffer (PB) pH 7.4. The brain was removed, fixed overnight with the same fixative, immersed in 30% sucrose in PB for cryoprotection for at least 48 h, and frozen in isopentane at −40°C. Cryostat brain sections (14-μm thick) were fixed in ethanol 70%, blocked with 3% normal serum, and incubated overnight at 4°C with primary antibodies: rabbit polyclonal antibodies against pan-laminin (1:100, #Z0097, Dako), P2RY12 (1:250, #AS-55043A, AnaSpec Inc.), or ionized calcium-binding adaptor molecule-1 (Iba-1) (1:100, #016-20001, Wako Chemicals), or mouse monoclonal antibody against myelin basic protein (1:200, BDI221, #ab66188, Abcam) followed by secondary antibodies (Alexa Fluor®; Thermo Fisher Scientific). Cell nuclei were stained with To-Pro3 (#T3605, Thermo Fisher Scientific). Images were obtained in a confocal microscope (TCS SPE-II, Leica Microsystems) with LAS software (Leica). Images were no further processed. Figures were prepared with Adobe Photoshop. When required for illustrative purposes contrast was enhanced globally in the whole image.

RNA Extraction

RNA was extracted from samples of FACS-sorted CD11c-eYFP^{+} cells, microglia, astrocytes and endothelial cells with PureLink RNA Micro Kit (#12183016, Invitrogen) following manufacturer indications with minor modifications. RNA was precipitated with 70% ethanol overnight at −20°C. To avoid genomic DNA contamination a DNase step was performed. RNA quantity and purity were assessed with the High Sensitivity RNA ScreenTape® (Agilent 2200 TapeStation system). We also extracted RNA from brain tissue using Trizol® Reagent (Life Technologies) followed by the PureLink RNA Mini Kit (#12183018A, Invitrogen). In this case, we assessed the RNA quantity and quality using a ND-1000 micro-spectrophotometer (NanoDrop Technologies).

RT-PCR

Total RNA was reverse-transcribed using a mixture of random primers (High Capacity cDNA Reverse Transcription kit, Applied Biosystems, Foster City, CA, USA, #4387406). For RNA obtained from brain tissue, 1000 ng of total RNA were reverse-transcribed and the final product was diluted 6 times in RNase-free water. For samples of FACS-sorted cells, cDNA was pre-amplified following the manufacturer indications (TaqMan® Pre Amp Master Mix (2 ×), #4384266, Thermo Fisher Scientific) in order to have enough cDNA for the real-time-PCR. The pre-amplification step was carried out using a pool of TaqMan probes of interest and the final pre-amplified product was diluted 20 times with tris-EDTA buffer pH 8.0 (#BP2473, Fisher Bioreagents).

Real-time quantitative RT-PCR analysis was carried out with Taqman system (#4304437, Thermo Fisher Scientific) using the iCycler iQTM Multicolor Real-Time Detection System (Bio-Rad). The primers are listed in Table S4 and the qPCR conditions were 2 min at 50°C, 10 min at 95°C followed by 40 cycles of 15 s at 95°C and finally 1 min at 60°C. Quantification was performed by normalizing cycle threshold (Ct) values with the housekeeping gene (Hprt1) Ct, and analysis was carried out with the $2^{-\Delta\Delta CT}$ method.

Transcriptomic analysis

RNA samples were obtained from sorted eYFP^{+} cells of the ipsilateral brain hemisphere of CD11c-eYFP mice 4 days post-ischemia, the spleen of control CD11c-eYFP mice and the ipsilateral brain hemisphere of the WT mice of parabiotic CD11c-eYFP/WT pairs, and from microglial cells sorted from control brain and the ipsilateral brain hemisphere 4 days post-ischemia of Cx3cr1Cre^{ERT2}:ROSA26-tdT mice. Samples had RIN values > 8.

For the first RNA-Seq comparison (i.e., CD11c-eYFP+ cells of ischemic brain, CD11c-eYFP^{+} spleen cells, CX3CR1^{+} microglia of control and ischemic brain), libraries were prepared using the TruSeq Stranded mRNA Sample Prep Kit v2 (#RS-122-2101/2, Illumina) according to the manufacturer's protocol. Briefly, from 2.4 to 147 ng of total RNA were used for poly(A)-mRNA selection using streptavidin-coated magnetic beads and were subsequently fragmented to approximately 300bp. cDNA was synthesized using SuperScript II reverse transcriptase (#18064-014, Invitrogen) and random primers. The second strand of the cDNA incorporated dUTP in place of dTTP. Double-stranded DNA was further used for library preparation. dsDNA was subjected to A-tailing and ligation of the barcoded Truseq adapters. All purification steps were performed with AMPure XP beads and eluted in 20 μl EB. Library amplification was performed by PCR on selected fragments using the primer cocktail supplied in the kit. Final libraries were analyzed using Agilent DNA 1000 chip to estimate the quantity and check size distribution, and were then quantified by qPCR using the KAPA Library Quantification Kit (#KK4835, KapaBiosystems) prior to amplification with Illumina's cBot. Libraries were sequenced Single Reads, 50nts on the Illumina HiSeq 2500.

For the second RNA-Seq comparison (i.e., CD11c-eYFP^{+} cells from ischemic brain, Parabiotic CD11c-eYFP+ cells from the ischemic brain of WT mice, CX3CR1^{+} microglia from ischemic brain), libraries were prepared using the SMART-Seq v4 Ultra Low

Input RNA kit (#634890, Clontech) and NEBNext Ultra DNA Library Prep kit (#E7370, New England) according to the manufacturer's protocol. Briefly, 1 or 5 ng of total RNA were converted to cDNA using the SMART-seq kit. Long distance PCR was performed for 9 (5 ng) or 11 (1 ng) cycles. Agilent 2100 Bioanalyzer (High Sensitivity DNA Chip) was used for quantification and validation of the obtained cDNA. Ten ng of the resultant cDNA was fragmented using the Covaris S2 instrument in a final volume of 55 μL and adjusting the settings as follows: 10% duty cycle, intensity 5, and 200 cycles per burst for 5 minutes. The resultant fragments were used for the library synthesis using the NEBNext Ultra kit. Briefly, fragments were subjected to end repair and addition of "A" bases to 3′ ends, ligation of adapters and USER excision. Library amplification was performed through 10 cycles of PCR using different indexed primers for multiplexing. All purification steps were performed using AgenCourt AMPure XP beads. Final libraries were analyzed using Agilent DNA High Sensitivity chip to estimate the quantity and to check the size distribution and were then quantified by qPCR using the KAPA Library Quantification Kit (#KK4835, KapaBiosystems). Sequencing was carried out using the Illumina HiSeq 2500, Single Reads, 50nts.

Raw reads were analyzed for data quality using FastQC v0.11.5 (Babraham Bioinformatics) and eventually filtered using skewer v0.2.2 (Jiang et al., 2014) for removing the low quality reads and trimming the Illumina adaptor if necessary. Reads were then aligned to the reference genome (GRCm38) using the annotation from Ensembl (version 88) with STAR aligner (v2.5.3a) using the option "quantMode GeneCounts" for retrieving the gene counts. Differential gene expression analysis was performed using DESEQ2 package (Love et al., 2014), while plots were made using R programming language. We considered as differentially expressed genes that showed a logFC > |1.5| and adjusted p value < 0.001.

ImmGen transcriptomic data comparison

We compared our transcriptomic data with defined ImmGen populations (https://www.immgen.org/) (Miller et al., 2012) following a methodology used in previous studies (Poczobutt et al., 2016), with modifications. The analysis was carried out by Anaxomics Biotech (Barcelona, Spain). In a nutshell, pairwise comparisons between 8 selected ImmGen populations were performed using the Population Comparison tool (http://rstats.immgen.org/PopulationComparison/). The 100 most differential genes in each pairwise comparison were retrieved and a single list of differential genes was generated. We examined the expression of these genes in the comparison between: (a) control brain microglia and control spleen CD11c-eYFP$^+$ cells, (b) microglia versus brain CD11c-eYFP$^+$ cells of ischemic mice, and (c) microglia versus parabiotic brain CD11c-eYFP$^+$ cells of ischemic mice. Genes without a valid value were removed. The expression values of the final lists of genes in each sample (transformed to a Z-score) were used to construct a heatmap representation and an unsupervised gene clustering analysis was performed. The latter analysis was then used for the identification of specific clusters that displayed a differential expression between the studied cohorts. The genes inside these clusters were retrieved and submitted to ImmGen's My Gene Set tool (http://rstats.immgen.org/MyGeneSet_New/index.html). Boxplot representations of the expression value (Log2 of the gene expression value/average expression value of all genes) per each analyzed population were retrieved.

Enrichment analysis

Functional analyses of RNA-Seq data were carried out through the use of DAVID Bioinformatics Resources 6.7 (Huang et al., 2009). Then a hypergeometric enrichment analysis was performed by Anaxomics Biotech to determine the presence of enriched pathways and protein sets in our different cell populations, following previously described methodology (Subramanian et al., 2005). We mapped from mouse genes annotated in the various comparisons of gene expression profiles above described to mouse protein entries according to UniProtKB (The UniProt Consortium, 2017). Genes included followed the criteria: p value < 0.001 and |Log2FC| > 2. The differential genes/proteins were submitted to hypergeometric enrichment analysis (one for each cell population and comparison) to identify the pathways and molecular processes more enriched in each of the cell cohorts (Rivals et al., 2007). Enrichment was run over the following databases: GO terms (Biological Process, Cellular Component, Molecular Function) (Ashburner et al., 2000), KEGG pathways (Kanehisa et al., 2017), pathological conditions and motives included in BED database (Jorba et al., 2020), PharmGKB pathways (Whirl-Carrillo et al., 2012), the pathways from Small Molecule Pathway Database (SMPDB) (Frolkis et al., 2010), and the regulatory molecular mechanisms included in TRRUST database. Cytoscape software v3.5.1 was used to create the representation of individual enriched protein sets based on their enrichment score (Shannon et al., 2003).

Quantification of middle cerebral artery anastomoses

A solution of the lipophilic carbocyanide dye, DiI (DiIC$_{18}$(3)) was prepared according to a reported protocol (Li et al., 2008). The animals were perfused with 20ml of PBS containing heparin (5 U/mL), 10mL of DiI solution and 10mL of PFA 4% diluted in phosphate buffer consecutively, all at a 5ml/min rate. The brain was removed from the skull, the cortex was dissected out and set on a glass slide for observation. Pictures were taken with an Olympus inverted visible light microscope at 20x and merged to reconstruct the whole cortex surface. Two independent investigators blinded to the genotype of the mice manually counted the number of anastomoses between the middle and the anterior and posterior cerebral arteries. The correlation between the two independent measurements was studied.

QUANTIFICATION AND STATISTICAL ANALYSIS

Two-group comparisons were carried out with two-tailed Mann–Whitney test or t test, as required after testing for normality, and adjusting for paired measures using Wilcoxon-matched-pairs signed rank test or paired t test. One-sample Wilcoxon test was used to compare with reference values. Multiple comparisons t test and Holm-Sidak method was used. Multiple groups were compared with one-way ANOVA or Kruskal-Wallis test, or two-way ANOVA, followed by appropriate post hoc analyses. In experiments designed to study differences between groups receiving drug treatment, sample size was calculated using G*power 3.1 software (University of Düsseldorf) with an alpha level of 0.05 and a statistical power of 0.8. The size effect (d = 1.1) was estimated based on information on the group mean and SD from previous flow cytometry data of our own laboratory. In experiments designed to study differences in infarct volume between genotypes, the size effect was estimated at 0.97 for a change of 30% based on prior information on infarct volume mean and SD for wild-type mice subjected to ischemia by the same researcher. We built from these numbers the number of animals needed for comparing other outcome measures. For measurements designed as proof of concept, validation, or as internal controls we used minimum reasonable numbers of animals for confirmatory purposes. The specific tests used in each experiment, p values, and n values are stated in Figure Legends. We used GraphPad Prism software version 8.2.0.